JOINT EUROPEAN TORUS

JET–P(91)12

H.P. Summers, W.J. Dickson, A. Boileau, P.G. Burke, B. Denne-Hinnov,
W. Fritsch, R. Giannella, N.C. Hawkes, M von Hellermann, W. Mandl,
N.J. Peacock, R. Reid, M.F. Stamp, P.R. Thomas
and JET Team

On Spectral Emission from Beryllium in Plasmas

On Spectral Emission from Beryllium in Plasmas

H.P. Summers, W.J. Dickson, A. Boileau[1], P.G. Burke[2], B. Denne-Hinnov, W. Fritsch[3], R. Giannella, N.C. Hawkes[4], M von Hellermann, W. Mandl, N.J. Peacock[4], R. Reid[2], M.F. Stamp, P.R. Thomas and JET Team*

JET-Joint Undertaking, Culham Science Centre, OX14 3DB, Abingdon, UK

[1]Tokamak de Varennes, Varennes, Quebec, Canada.
[2]Department of Applied Mathematics, Queens University, Belfast.
[3]Hahn-Meitner Institute, Glienicker Strasse 100, Berlin, Germany.
[4]Culham Laboratory, UKAEA, Abingdon, Oxon, OX14 3EA.
** See Appendix 1*

Preprint of Paper to be submitted for publication in
Plasma Physics and Controlled Fusion

Abstract

Spectral observations of ions of beryllium in the JET plasma are described and are interpreted in terms of the interplay of atomic reactions and local plasma conditions. The methods of generalized-collisional-radiative theory are extended and used to provide a quantitative model. Emphasis is placed on the role of metastable ion states. The diagnostic scope of beryllium observations is explored for the influx ions Be^{+0} and Be^{+1} in the visible spectral range, for Be^{+2} in the XUV, and for Be^{+3} by charge exchange spectroscopy. Useful results for general diagnostic interpretation are presented in tables and graphs. The calculation procedures and data form part of the 'Atomic Data and Analysis Structure' in use at JET.

1. Introduction

In 1989, a major experiment was initiated in the JET Tokamak to assess the effectiveness of beryllium as the surface material contacted by the plasma.

As part of the diagnostic effort in the experiment, spectroscopic measurements were carried out covering extended spectral regions. These included visible observations along lines of sight to selected limiting surfaces and lines of sight through neutral beam penetrated plasma as well as fixed radial horizontal chord integrated spectral measurements in the VUV/XUV. It transpires that beryllium reveals a number of remarkable features in its spectrum, not previously reported. The diagnostic scope of these is much richer than had been anticipated, but requires some elaboration of existing atomic modelling for its exploitation. This paper is concerned with interpreting these spectral observations, an explanation of the associated atomic physics calculations and presentation of useful derived quantities. Details of deduced plasma performance in JET during the beryllium experiments, which draw on a much more extended range of diagnostics are described elsewhere (Thomas, 1990).

The study of beryllium divides naturally into three parts, namely,

(a) Be^{+0} and Be^{+1} which only occur near the plasma boundaries and are inflowing in an ionising environment. They are conveniently observed in the visible/quartz uv regions;

(b) Be^{+2} and Be^{+3}, which are more extended in occurrence and radiate primarily in the XUV region. They are also possibly in a state of flux;

(c) Be^{+4}, the generally occurring ionisation stage at high temperatures but which is illuminated (by conversion to Be^{+3}) by the charge transfer reaction from neutral deuterium in beam penetrated plasma.

In section (2), the spectral phenomenology of each part is described together with a qualitative assessment of the underlying reaction kinetics. In section (3) the atomic physics models are addressed in more detail. Section (4) is concerned with quantitative discussion of the diagnostic opportunities identified in the previous sections. The summary conclusions are in section (5).

2. Spectral Phenomenology

2.1 The Influx Ions Be^{+0} and Be^{+1}

Neutral and near neutral ions occur in the extreme periphery of the plasma close to the surface which is their source. Some general techniques for interpreting spectral emission along lines of sight directed at surfaces for inflowing light ions of carbon and oxygen in terms of total impurity flux have been described by Behringer *et al* (1989) (hereafter called paper I). In principle, we have the same objectives for the beryllium ions. Be^{+0} is the initially released species from the surface (or initial product of molecular catabolism). Its energy level structure is shown in figure 1. Be^{+0} has singlet and triplet spin systems, $2s^2\ ^1S$ being the ground state and $2s2p\ ^3P$ a metastable state. Prior to the JET beryllium experiment, surveys were carried out on the ISX-B (Isler *et al.*, 1985) and UNITOR (JET internal memo, 1989) devices on suitable spectral lines for measurement. The UV lines at 3321Å, 2651Å and 2495Å on the triplet side and 2348Å on the singlet side are prominent radiators. To assess the total beryllium flux from Be^{+0}, in the manner prescribed in paper I, requires separate singlet and triplet line measurements and this is indeed necessary since there is evidence on ISX-B and UNITOR that the metastable to ground population ratio varies significantly with plasma conditions.

On JET however, signals are transferred by long (circa 150m quartz fibres) to remote detectors which restricts measurement to long wavelengths (> 3500Å). The 3321Å line is strongly attenuated. The higher n-shell transition at 6786Å is very weak and so there is no line suitable for observation at JET on the triplet side of Be^{+0} - a serious limitation. Assessment of the total beryllium flux from Be^{+0} is not possible on JET, but only the singlet flux. A number of longer wavelength lines can be measured on the singlet side and therefore in principle used for this, such as 8254Å, 4408Å and 4573Å.

However, figure 2 is revealing. It shows the ratio of 4408Å and 8254Å emission in a series of JET limiter measurements as a function of line averaged electron density. If local edge density relates directly to line averaged electron density (an assumption not fully justified since local temperature and density are connected by the efficiency of power radiation by impurities at the plasma periphery), then this is a density sensitive line ratio. We examine this ratio in detail in section 4.1.

The electron temperature at the region where Be^{+0} emits appears from probe studies to be ~30eV. This is evidently not the natural temperature at which Be^{+0} radiates in non-diffusive equilibrium (T_e~3 eV is more typical) so the Be^{+0} atoms are penetrating to that temperature environment on a timescale less than or equal to the ionisation timescales. The high temperature, highly ionising regions in which the Be^{+0} finds itself in turn allows an imbalance in the ground to metastable population ratio to develop. The diagnostic opportunity of this is also explored in section 4.1.

Be^{+1} is by contrast a simpler ion. Its term diagram is shown in figure 3. There is a single (doublet) spin system and 2s ^2S is the ground state.The fundamental resonance lines 2s $^2S_{1/2}$-2p $^2P_{1/2, 3/2}$ at 3131.06Å and 3130.41Å are the most intense lines in the beryllium spectrum, but are (as for the short wavelength Be^{+0} lines) strongly attenuated in the JET optical system. Transitions between n=3 and 4 principal quantum shells are therefore the most useful for observation and include 5270.7Å, 4360.9Å and 4673.5Å. Any of the Be^{+1} lines is therefore a potential monitor of the total Be^{+1} and therefore total beryllium flux. Figure 4 shows the ratio of the emission in Be II (4361Å) and Be I (8254Å) as a function of line averaged density. This ratio, with some adjustments for local temperature and density, might be expected to be an indirect measure of the Be^{+0} triplet to singlet flux ratio.

2.2 The Plasma Ions, Be^{+2} and Be^{+3}

Figure 5 shows a portion of the XUV spectrum as observed along a horizontal line of sight directed radially at the inner wall of JET in the mid-plane. The plasma was in contact with the outer belt limiters at the time of the measurement. Attention is drawn to the $1s^2\ ^1S_0$-1s2p $^1P_1$ resonance line of Be^{+2} at 100.26Å together with its higher series members $1s^2\ ^1S_0$ - 1snp$^1P_1$ with n up to 8 resolvable, and the 1s ^2S - 2p ^2P resonance line of Be^{+3} at 75.93Å. The higher Lyman series members of Be^{+3} were not used in the presently reported JET study. The relative intensities of Be^{+2} series members are quite sensitive to particular plasma conditions. In a cooling discharge in contact with the inner wall, we have strong evidence of charge transfer from thermal neutral deuterium as a populating mechanism for the upper levels of the higher series members. This is similar to the situation analysed by Mattioli *et al.*, (1989) in C^{+5}, and will be described in a further work. It will be shown that the present decrement

indicates Be^{+2} to be an inflowing ion with collisional excitation from the ground state $1s^2\ ^1S$ followed by cascade responsible at least for the low series members up to n=4. The relative intensities of members then depend on the local electron temperature.

The intersystem line $1s^2\ ^1S_0$ - $1s2p\ ^3P_1$, at 101.69Å has been observed for the first time although its wavelength has been anticipated theoretically and semi empirically (eg. Drake, 1988; Edlen 1952) on a number of occasions. Our measured wavelength at 101.695 $\pm$ 0.015Å measured relative to Be III 100.2552Å (Svensson, 1970) and CVI 33.7360Å in third order (Garcia & Mack, 1965) is insufficiently precise to contribute to theoretical discussions although it is consistent with them. The associated branching multiplet $1s2s\ ^3S$-$1s2p\ ^3P$ occurs in the quartz UV at 3721-3723Å and is shown in figure 6. Note that the $1s2s\ ^3S_1$ - $1s2p\ ^3P_1$ component is well resolved and so provides a pure branch with the XUV intersystem line. Also the summed $^3P_2$ and $^3P_0$ components are twice the $^3P_1$ components as expected since the intersystem branch gives only a small (~1/100) correction to the $^3P_1$, radiative lifetime. Intensity calibration in the XUV has been troublesome at JET due to short and long period variation of detector sensitivity particularly at the positions of strong spectrum lines. The present observations and some associated modelling help in the resolution of this problem. The intersystem to resonance line intensity ratio is related to the metastable to ground population ratio and can indicate diffusive imbalance. This is similar to the Be^{+0} case and is examined in section 4.2.

2.3 Charge Exchange Spectroscopy of Be^{+3}

Figures 7a and 7b show the spectral range from 4640Å - 4720Å as observed along a vertical viewing line intersecting the neutral deuterium heating beams at approximately the plasma centre when the beams are active and inactive, respectively. The feature at 4658.5Å is the high principal quantum shell transition Be IV (n=6-5). Without beams it is only emitted towards the periphery of the plasma (cf. section 2.2). With the beams active, a large broad feature is superimposed resulting from Be IV (n=6-5) emission at the beam/viewing line intersection in the core of the plasma. It is excited by the charge transfer reaction.

$$D_{beam}(1s) + Be^{+4} \rightarrow D^{+} + Be^{+3}(nl)$$

Detailed attention has been given to the charge exchange spectroscopy (CXS) of other light impurities in JET (Boileau *et al.*, 1989) and similar analysis is enabled by this observation. After subtraction of the unavoidable peripheral component in the line of sight by multiple Gaussian techniques, the width and displacement of the residual charge exchange feature indicates ion temperature and plasma rotation. The width of the charge exchange feature is to be contrasted with that of the nearby Be II line at 4673.5Å. This narrow plasma edge emitted line (assumed therefore non-rotating) is an advantage for CXS of beryllium since it provides a wavelength reference for rotation measurements.

A problem is presented at 4685.2Å. In the pre-beryllium operation, this feature was due to helium present as an added minority species for radio-frequency energy coupling. It was routinely used to monitor helium. The He II (n=4-3) line and vicinity is also expected to be important for measuring slowing down and thermalised alpha particles formed by deuterium/tritium fusion in the late active phase of the JET experiment. Slowing down alpha particles are expected to produce a weak, very broad (~100Å) feature. There is, however, an unavoidable wave-length coincidence with the Be IV (n=8-6) transition. So the feature at 4685.2Å is in general now a superposition of helium and beryllium emission. On the other hand, the ratio of the charge exchange induced emissivities of BeIV 4658.5Å and BeIV 4685.2Å is a function of independently known plasma and beam parameters and so predictable theoretically. Therefore the separate contributions to the 4685.2Å feature are in principle resolvable with the 4658.5Å line providing an intensity reference for rotation measurements.

It is evident that beryllium as an impurity in JET can be used diagnostically in all regions of the plasma. A comprehensive 'collisional-radiative' approach to the theoretical atomic modelling is essential along with a suitable quality basis of fundamental atomic collision data for full exploitation.

3. Atomic Physics Aspects

3.1 Model Development

The calculation of the quantities called the 'ionisation per emitted photon' has been described in paper I. To summarise the main points of that work, the flux of an element A, Γ^A, can be obtained by measurement on any of its ions, for example A^{+Z}, through which A ionises completely local to the surface without

dispersive or return losses and that this flux is composed of effectively independent fluxes in each of the metastable states of A^{+Z}, that is A_ρ^{+Z} : ρ=1, ..., m so that

$$\Gamma^A = \sum_\rho \Gamma\left(A_\rho^{+Z}\right)$$

('metastables' denote both ground and metastables in this notation). These component fluxes can be expressed in terms of the observed line of sight integrated emissivities of m spectrum lines, I_σ, which are linearly independent and characterise the metastable populations as

$$\Gamma\left(A_\rho^{+Z}\right) = \sum_\sigma P_{\rho\sigma} I_\sigma$$

The P's are the generalisation of the 'ionisation per photon' quantities. If the spectrum line σ corresponds in fact to a transition i-j between excited levels of A^{+Z}, then determination of $P_{\rho\sigma}$ requires deduction of that part of the population of level i which depends on metastable ρ, and the effective ionisation rate coefficient from metastable ρ, S_ρ. Note that the population of level i, $N_i^{(Z)}$ might be written formally as

$$N_i^{(Z)} = \sum_\rho = N_e F_{i\rho} N_\rho^{(Z)}$$

The F's are derived theoretically. However the present study requires an extension of the calculations of paper I for $N_i^{(Z)}$ and S_ρ. The reason is evident from the influence of different processes with increasing density on those excited level populations which lead to observed emission, namely

(a) Low density - collisional excitation from ground and and metastable levels only, radiative cascade. Direct ionisation and excitation autoionisation only.

(b) Moderate density - collisional excitation amongst a complete set of low levels, (especially nearby degenerate levels), radiative cascade.

Direct ionisation and
excitation/autoionisation only

(c) High density - Collisional excitation amongst low levels, excitation to and amongst highly excited levels. Influence of highly excited levels on low levels. Direct ionisation, excitation/autoionisation and ionisation from excited states.

The boundary for the different density regions depends on the ion structure and also on ion charge. Approximately, $N_e/(Z+1)^7 \sim 10^{12}$ cm^{-3} marks the (a)/(b) boundary and $N_e/(Z+1)^7 \sim 5 \times 10^{12}$ marks the (b)/(c) boundary. For Z=1, 2 as examined in Behringer *et al* (1989), solution in the (a) and (b) approximations is appropriate for the tokamak edge, but for Z=0, case (c) must be applied. It should be added that equation (1) and the discussion above applies to an ionising situation. Recombination, either by free electron capture or charge exchange can be included in a full description as

$$N_i^{(Z)} = \sum_{\rho} N_e F_{i\rho} N_\rho^{(Z)} + \sum_{\tau} N_e R_{i\tau} N_\tau^{(Z+1)} + \sum_{\tau} N_D C_{i\tau} N_\tau^{(Z+1)}$$

where their respective contributions $R_{i\tau}$ and $C_{i\tau}$ are again derived theoretically. Reference has been made to low excited levels and highly excited levels and it is appropriate to make this separation at the principal quantum shell which includes the highest lying observed transition upper state. In Be^{+0}, $2 \leq n \leq 4$ constitute the low level group and $4 < n < \infty$ the high level group.

There is a simplification. The highly excited level populations may be considered for whole principal quantum shells since collisional processes fully mix sub-levels of the same principal quantum shell. This is called a 'bundle-n' viewpoint (Burgess & Summers, 1986). The calculation procedure for case (c) is as follows: A bundle-n calculation is performed on each recombined ion (Z) spin system and recombining ion (Z + 1) metastable state, but excluding direct collisional or radiative couplings for n and n′ belonging to the low level group. The solution generates a set of projected indirect couplings between n and n′ belonging to the low level group. These can be expanded using statistical weight factors over the resolved low level group (that is separated into terms or levels) and combined with the detailed direct couplings. Only this latter part was used

in paper I. On solution, the resolved low level populations include the influence of the high levels and all ionisation pathways as well as recombination. The influence of the resolved low level populations can in turn be projected on the metastable levels yielding effective ionisation coefficients including all stepwise processes. We term this progressive condensation (see Summers and Hooper, 1983) and it is summarised in figure 8.

This full procedure is necessary for the study of Be^{+0}. The low level group is $2 \leq n \leq 4$ and the resolved low level group is all the levels shown in figure 1. The metastable states are $2s^2\ ^1S$ and $2s2p\ ^3P$. There are two spin systems and a single recombining ion metastable state, namely $2s\ ^2S$.

The moderate density approach is appropriate for Be^{+1} and Be^{+2}.

For charge exchange spectroscopy studies of Be^{+4}, the effective emission coefficients are obtained by the procedures described in Boileau *et al.* (1989) and Summers *et al.* (1991). These works are comprehensive and no further details are presented here.

3.2 Fundamental Atomic Data

Energy levels for Be I are taken from Bashkin and Stoner (1978) and oscillator strengths from a number of sources including Wiese, Smith and Glennon (1966) Weiss (1972), (but note the corrected position of $2p^2\ ^1S$) Fawcett (1984) and Cohen and McEachran (1979). The very small oscillator strengths for the $2s^2\ ^1S$ - $2s3p\ ^1P$ and $2s^2\ ^1S$ - $2s4p\ ^1P$ transitions are of note. The $2s3d\ ^1D$ and $2s4d\ ^1D$ terms are relatively high lying because of the series perturbation by $2p^2\ ^1D$. Also of note is the unusually large oscillator strength for $2s^2\ ^1S$ - $2p3s\ ^1P$ (a two electron transition). Since $2p3s\ ^1P$ lies in the 2s continuum, and can autoionise, it is probably not a significant contributor to $2s3s\ ^1S$ by cascade. Only simple approximations for electron impact excitation cross-sections have been available for Be^{+0} up until now. As part of this study, new 12 state and 20 state R-matrix calculations have been carried out. Details are presented in Fon et al. (1991). Effective potential Born calculations (see paper 1) for $2s^2\ ^1S$ - $2s3s\ ^1S$, $2s^2\ ^1S$ - $2s4s\ ^1S$ and $2s^2\ ^1S$ - $2s3d\ ^1D$ coefficients are 30%, 32% and 300% greater respectively than the new values at Te= 20eV. This justifies our avoidance (based on uncertainty of the series perturbation influence) of the $2s2p^1\ p$ - $2s3d\ ^1D$ spectral line in our preliminary studies on UNITOR. Lines from $2s3s\ ^1S$ and $284s\ ^1S$ were

preferred. Progressively larger differences occur at low temperatures as expected. The new data is therefore essential in the trend to seek to diagnose low temperature high density plasma in divertors. Also of note are the quite large spin changing rate coefficients. These affect influx interpretation and are discussed in section 4. This was not explored in preliminary work since realistic spin changing cross-sections were not available. Two corrections to the rate coefficients are appropriate since explicit reference to configurations 2p3ℓ and 2p4ℓ has not been made (see the resolved low level group in figure 1). This is most significant on the triplet side, since such states are directly excitable from the 2s2p ^{3}P metastable and since the 2s3p ^{3}P level is semi-metastable. The overwhelming radiative decay (if it occurs in preference to Auger break up) of 2p3ℓ and 2p4ℓ is by transition of the inner 2p electron to 2s.Therefore excitation to 2p3s and 2p4p contribute to the effective excitation to 2s3s and 2p3p contributes to that of 2s3p. The direct rates from the metastable are adjusted for the maximum contribution from this. In fact the radiative decay path from 2s3p also must be through the 2s3s ^{3}S term but this is treated explicitly in the resolved low level group population calculation.

The energy level and oscillator strength data for BeII are well established. As for Be I, refined electron impact data are not available for the n=3 and 4 shells required in this study. For the 2s ^{2}S - 2p ^{2}P transition, there is the well known benchmark study (Hayes et al., 1977). We have carried out new calculations in the distorted wave approximation using the codes developed at University College, London (Eissner-unpublished) for all singly excited terms up to the n=4 shell. For 2s ^{2}S - 2p ^{2}P, the distorted wave result for the Maxwell averaged rate coefficient is 11% below experiment at 1.7 eV and within 4% of the close coupling theory at 345 eV. Note that the experimental data is not corrected for cascade. Good comparative data is not available for higher transitions. Deviation from dipole allowed impact parameter rate coefficients are typically 40% at Te~30eV. ℓ-state mixing cross-sections are evaluated in the impact parameter approximation.
At low density, cascade corrections to the effective excitation of high n shells and higher angular momentum states are appropriate, the strategy here depending upon whether the projection techniques are used (see section 4).

For Be III, the present study requires LS resolved energy levels, A-values and cross-section data up to the n=5 shell. Term centroid energies and A-values (for non spin changing $\Delta n>0$) are well known.

The level structure 1s2s ^{3}S and 1s2p ^{3}P and their radiative decays on the other hand have been the subject of detailed study. Table 2 summarises relevant data used here. The uncertainty bounds are from the spread of the data sources recorded and the preferred source underlined. These data imply that the branching ratio

$$\frac{A_{2^3P_1-2^3S_1}}{A_{2^3P_1-1^1S_0}} = 84.4\ (+5.8\ /\ -3.6)$$

Collision cross-sections are taken from the Coulomb-Born calculations of Sampson *et al.* (1984). Note that this data extends to Be^{+2} but the caveat relating to Z_0/N probably remains true.

The atomic data needs for Be^{+3} for this study are very different. It is charge exchange data which is required and for this, we have followed closely the approach used for helium, carbon and oxygen in earlier studies. Explicit nℓ-shell selective CX data for the reaction

$$D(1s) + Be^{+4} \rightarrow D^{+} + Be^{+3}(n\ell)$$

has only been available from Ryufuku (1982) in the range 10 keV/amu $\leq$ E $\leq$ 200 keV/amu. It is well known that this data underestimates at low energies for higher n-shell subdominant capture. New close coupled atomic orbital calculations are in progress (W Fritsch) and preliminary results have been used together with Ryufuku (1982) and parametrisations of the n-shell and nℓ-shell dependence of the partial cross-sections (Von Hellermann et al., 1991) to establish our current preferred charge exchange data set.

4. Theoretical Results and Discussion

4.1 $\underline{Be}^{+0}$ and $\underline{Be}^{+1}$

Note that because of the relatively large spin changing transition to excited states, singlet line emission has a contribution from excitation from the triplet metastable. It will be shown later that except at low temperature, the

Be^{+0} 2s 2p ^3P population is likely to be reduced in transient ionisation. For simplicity in the discussion and figures, only line emission arising from excitation from the lowest level of the same spin system is shown.
Following the full density dependent calculation described in section 3, figure 9a shows the 'ionization per photons' results for Be I 8254Å, a transition originating in the n=3 shell, which is our preferred spectrum line for characterising the singlet side flux of Be^{+0}. The electron temperature and electron density dependence implies that reasonable knowledge of these quantities at the BeI emission zone is required for flux deduction although the sensitivity is less for T_e>20eV and $N_e < 3x10^{12}$ cm^{-3}. These constraints are generally satisfied for JET limiter sources (as indicated by Langmuir probe measurements extrapolated to the last closed flux surface) but will not be for cool divertor sources. Figure 9a is to be contrasted with figure 9b for Be I 4408Å, a transition originating in the n=4 shell, for which the density dependence is greater (as anticipated in section 1). The reason is that the upper levels of the 8254Å and 4408Å transitions are 2s3s^1S and 2s4s^1S respectively. The latter is more susceptible to further exciting and ionising collisions with plasma electrons than the former. At densities $N_e \geq 2x10^{12}$ cm^{-3} for Be^{+0}, the disturbance of the 2s4s^1S population is quite significant. In this respect, at tokamak densities, neutral atoms are much more sensitive than ions, N_e/Z_1^7 with Z_1, the ion charge plus one, is the relevant scaled electron density parameter from 'collisional-radiative' theory (see Bates *et al.*, 1962). Note that in paper I collisional mixing amongst low levels was included, but not the processes resulting in ionisation operative in Be^{+0}. That was possible because of the restriction to the positive ions of light elements. Variation of the Be I 8254Å/Be I 4408Å emissivity ratio with T_e and N is shown in figure 10. For T_e >10eV, the ratio is predominantly N_e dependent, that is, it provides a weak N_e indicator at the Be I emission zone. Sufficient observational data for a systematic experimental study on this issue are not yet available. The data of figure 2 indicates the expected trend but the two spectrum lines were observed on different belt limiters and so the absolute value of the ratio is uncertain. Table 2a summarises the theoretical 'ionisation per photon' results for Be I 8254, 4408 and 4573 for completeness. Measurement of the short wavelength 3321 Å line on the triplet side will be possible in the next operation period of JET along a single vertical line of sight.

Table 2b summarises the theoretical 'ionisation per photon' results for Be II 3130.6, 5270.7, 4673.5 and 4361 Å lines calculated in the moderate density approximation but with cascade corrections (cf. paper I). Although collisional

mixing amongst populations of n=4 sublevels is expected to occur, the strong density sensitivity at moderate density of the Be^{+0} case is not anticipated because of the Z scaling of the critical electron density. Derivation of Be^{+1} flux using the tabulated photon efficiencies again requires some knowledge of T_e at the Be^{+1} zone, although the sensitivity to N_e is less than for Be^{+0}. Comparative observations have been made of the 4674 Å line originating from the 4f ^2F level, and of 5271 Å originating from the 4s ^2S level. The calculated emissivity ratio at $N_e = 5x10^{12}$ cm^{-3} and T_e = 25eV is 3.0. The observed experimental ratio variation in JET pulse #23249 was 3.4-4.4 at uncertain local temperatures and densities.

The evolution from Be^{+0} to Be^{+1} in an ionising, plasma is mediated by the effective rate coefficients shown in figure 11, that is, the separate generalised collisional-radiative ionisation coefficients for the ground and metastable state and the cross-coupling coefficient (treated as an electron impact rate) between metastable and ground. The ionisation rate coefficients increase with N_e due to the stepwise excitation/ionisation losses via excited states which influenced the Be^{+0} photon efficiencies. The cross-coupling coefficient has the opposite dependence on N_e and falls with T_e due to its spin changing nature. The tendency of ground and metastable populations of Be^{+0} to 'freeze' as at birth from the surface therefore is expected to develop if the Be^{+0} ionisation zone temperature advances above T_e ~10eV. Comparison of Be^{+0} (singlet) and Be^{+1} (total) flux at low density (which implies penetration of Be^{+0} to a higher temperature ionisation zone), although somewhat uncertain because of lack of detailed temperature knowledge, are approximately equal for the observational data of figure 4, suggesting that Be^{+0} enters the plasma in its ground state. At higher line averaged density, and therefore lower temperature at the Be^{+0} ionisation zone, the Be^{+0} (singlet) flux ratio appears to fall indicating progressively greater metastable Be^{+0} presence. This is not a birth process but a redistribution of Be^{+0} population from ground to metastable in the plasma. Evidently a full assessment of theory and experiment requires a spatial edge density/temperature/influx speed model.

This discussion has centred on transiently ionising influx aspects, but there is a further issue relevant to planned studies of cool high density divertor plasma. In steady state ionisation balance at T_e ~ 10eV, the dominant ionisation stage by a large factor is Be^{+2}, the helium-like stage. The dominant line radiation is however from the resonance line of the Be^{+1} stage since the electron temperature is too low to excite the Be III spectrum. The charge transfer reaction

from neutral hydrogen (deuterium) to Be^{+2} forming Be^{+1} at thermal energies is large. Therefore the presence of a dense neutral hydrogen cloud can markedly increase the total radiative losses even though the Be^{+1} fractional abundance remains small. In these circumstance, charge transfer can also affect transient ionisation development and necessitate modification of the simple interpretation of photon efficiencies in terms of impurity fluxes. Detailed calculations show the importance of precise time constants for diffusion and atomic processes and the necessity of a complete edge plasma model. Results of this will be published in due course.

4.2 $\underline{Be}^{+2}$

The moderate density calculation of the excited populations of the Be^{+2} has been performed including all levels of principal quantum number ≤ 5. Also, ionisation rate coefficients for the ground state $1s^2\ ^1S$ and the metastable state $1s2s\ ^3S$ have been computed together with the collisional-radiative cross-coupling coefficients between $1s^2\ ^1S$ and $1s2s\ ^3S$. Consider firstly the singlet series $1\ ^1S - n\ ^1P$. Figure 12 shows calculated emissivity ratios to $1\ ^1S - 2\ ^1P$ of the members with n = 3 and 4 as a function of T_e. The curves superpose for densities over the range $N_e \leq 5x10^{13}$ cm^{-3}. For $T_e \leq 50$ eV, the ratios are quite sensitive to T_e (due to exponent factors in the excitation rate coefficients). We draw attention again to the intersystem line $1\ ^1S_0 - 2\ ^3P_1$. Excitation to $2\ ^3P_1$ from $2\ ^3S_1$ exceeds that from $1\ ^1S_0$ by a factor > 30 in all circumstances. As for the ionisation of Be^{+0}, we can explore the limiting case of time - dependent ionisation from an initial ground state Be^{+1} ion through Be^{+2} and Be^{+3} in a plasma of fixed T_e and N_e. The rate coefficients do not depend significantly on N_e, so N_e merely acts as a scaling factor of the ionisation times. The time integrated emissivity ratio of $1\ ^1S_0 - 2\ ^3P_1$ and $1^1S_0 - 2^1P_1$ is shown in figure 13 and is contrasted with the equilibrium ratio. The observed ratio in JET is typically ~ .05 suggesting that Be^{+2} has penetrated to a high temperature ionisation zone ~ 250 eV and the transiently ionising picture is appropriate.

It is apparent that the microchannel plate detector used in the grating incidence XUV spectrometer on JET shows pronounced sensitivity variation in wavelength and time. The principal effect appears to be a reduction in sensitivity at the positions of strong lines (called 'gain fatigue') which depends amongst others on irradiation history and duration from last exposure to atmosphere. Therefore, in the more detailed assessment of theory and

observation, we seek to comment on intensity calibration as well as diagnostics. Systematic comparisons of the Be III 1^1S - n^1P series and 1^1S_0 - $2\,^3P_1$ in the XUV spectrometer with the $1\,^1S$ - $2\,^1P$ line observed in a nearly collinear (within 8°) VUV instrument indicates that 'gain fatigue' is not present or at least small for weak lines and in particular for $1\,^1S$ - 4^1P and 1^1S_0 - $2\,^3P_1$. On the limiting highly ionising model, the predicted ratio of emissivities of these lines is also shown in figure 13. Evidently the ratio is a sensitive T_e diagnostic. Results for typical cases such as illustrated in figure 5 give $T_e \sim 250$ eV. At this temperature the theoretical emissivity ratios $1\,^1S$ - 3^1P/ 1^1S - 2^1P and 1^1S - 4^1P/1^1S - 2^1P are determined as 0.15 and 0.035 respectively. These differ from the immediate observations before 'gain fatigue' correction. Development of 'gain fatigue' by the XUV spectrometer is shown in the comparative data for many pulses of figure 14. The early pulses are believed to show little 'gain fatigue'. The corrected observed ratios are then probably ~ 0.16 and ~ 0.04 respectively. This result gives some support to the theoretical model and also suggests that the model may be used in support of relative calibration over the extent of the singlet series in the XUV. As pointed out in section 1, the branching line pair 1^1S_0 - 2^3P_1 and $2\,^3S_1$ - $2\,^3P_1$ provide an absolute calibration transfer to the 100 Å region from a calibrated quartz UV position. (Note however the uncertainty in the theoretical branching ratio). This is provided the plasma is optically thin, (the situation in JET) and satellite lines are negligible (also true). Be III emission is therefore a transient ionisation and electron temperature indicator and provides in association with theory, a contribution to intensity calibration in the XUV.

4.3 $\underline{Be}^{+3}$

The effective emission coefficients, q, for Be IV n=6-5 and Be IV n=8-6 are shown in figure 15 for one representative set of plasma parameters following charge transfer from D(1s). The photon emission/cm^3/sec is therefore $N_{Be^{+4}}^{Plasma}\, N_{D(1s)}^{beam}\, q$. Redistribution and cascade combined with the initial distribution of direct capture determines the effective coefficients. The availability of two closely neighbouring observable spectrum lines with different upper principal quantum shells is an advantage, since it allows some critical judgement of the theory and fundamental cross-section data. Time histories of the two spectrum lines in discharges with low helium are the same and deduced beryllium ion temperatures from them are in very close agreement. This suggests that interpretation of the 4685 Å line as Be IV n=8-6 in these circumstances is sound.

The deduced beryllium density from the two lines surveyed over a number of discharges is more variable. For typical, fairly low ion temperature conditions (see for example figure 15), the theoretical effective emission coefficient ratio is ~ 5.5.

A careful analysis of the line ratio for such a case, using a beam modulation method for elimination of background and plasma edge radiation indicates an experimental ratio ~ 5.2. Although the agreement is satisfactory, at high plasma ion temperatures, accurate charge exchange spectroscopy deductions need good knowledge of the effective emission cross-sections over a fairly wide range of energies about the beam energy. It is not yet clear that our preferred theoretical data is reliable for high subdominant levels at energies significantly below 40 keV/amu.

The JET beryllium experiment had three parts, namely: (i) a pre-beryllium carbon phase, (ii) a beryllium evaporation phase and (iii) a beryllium limiter phase. Tracing of the dominant impurities (i.e. carbon and beryllium) by charge exchange spectroscopy through these phases was possible. A transition from pure carbon impurity to almost pure beryllium impurity dominated plasmas were observed and reconstruction of Z_{eff} from the impurity densities performed. An evaporation phase illustration of the comparison with Z_{eff} from visible bremsstrahlung is shown in figure 16 during which there were pronounced impurity density variations. The good agreement is a strong validation of overall charge exchange spectroscopy analysis on JET. For completeness, table 3 summarises our current effective emission coefficients for BeIV n =6-5.

5. Conclusions

A review has been presented of the range of spectroscopic observation available from beryllium in the JET experiment. These data have been shown to allow comment on impurity flux from surfaces, local electron temperature, electron density and transiently ionising conditions near the plasma periphery, ion temperature and impurity concentrations in the bulk plasma.

Collisional-radiative modelling of excited level populations, spectral emission and ionisation of all beryllium ions has been carried out. Extensions to allow detailed study of neutral atoms, high density environments, transient conditions and the role of metastables have been made.

Observation of the Be III $1s^2\ ^1S_0$ - $1s2p\ ^3P_1$ intersystem line is reported for the first time. A valuable branching ratio for XUV spectrometer calibration has been identified.

Techniques presented and evaluated in this paper are of direct relevance to impurity studies in cool, dense divertor plasmas. The diagnostic opportunities of other light impurities such as B, C and 0 are expected to be comparable to those of Be.

Extensive atomic data have been used and some new calculations have been carried out. It is hoped that the paper will stimulate further special studies. New Be^{+4} charge exchange cross-section calculations are in progress and revised tables will be supplied in due course. Only a limited portion of the photon efficiency data has been presented and further details are available from the authors.

Acknowledgements

Valuable discussions took place with Professor J Hackmann. The opportunity to carry out preliminary studies of beryllium spectra on the UNITOR tokamak at the University of Dusseldorf are gratefully acknowledged. HPS and WJD are on contract from the University of Strathclyde.

References

S BASHKIN, J O STONER, (1978) 'Atomic Energy Levels and Grotrian Diagrams' (publ., North Holland).

D R BATES, A E KINGSTON, R W P MCWHIRTER (1962)
Proc. Roy. Soc. A267, 297.

K BEHRINGER, H P SUMMERS, B DENNE, M FORREST, M, STAMP (1989)
Plasma Physics and Controlled Fusion 31, 2059.

K L BELL, H B GILBODY,J G HUGHES, A E KINGSTON, F J SMITH (1982)
Culham Laboratory Report CLM-R216.

A BURGESS, H P SUMMERS (1987)
Mon. Not. R. Astr. Soc. 226, 257.

M COHEN, R P McEACHRAN, (1979)
J Quant. Spectros Rad. Transfer 21, 1.

G W F DRAKE (1988)
Can. J. Phys. 66, 586.

B EDLEN (1952) Ark. Fys. 4, 441.

B C FAWCETT, (1984)
At. Data and Nuclear Data Tables 30 426.

W C FON, K A BERRINGTON, P G BURKE, A HIBBERT (1991)
J. Phys. B - submitted.

M J FORREST, J HACKMANN, N J PEACOCK, M F STAMP, H P SUMMERS (1989) JET Internal Memorandum.

J D GARCIA, J E MACK (1965)
J. Opt. Soc. Am. 55, 654.

M A HAYES, D W NORCROSS, J B MANN, W D ROBB (1977)
J. Phys. B 10, L429.

M VON HELLERMANN, W MANDL, H P SUMMERS, A BOILEAU, R HOEKSTRA, F J DE HEER, J FRIELING
(1991) Plasma Phys. Cont. Fusion - submitted.

R C ISLER, K BEHRINGER, et al (1985) Nuclear Fusion 25 1635.

H RYUFUKU (1982)
Japan Atomic Energy Research Institute Report, JAERI-M-82-031.

D H SAMPSON, S J GOETT, R E H Clark (1983).
At. Data Nucl. Data Tables 29, 467.

J SPENCE, H P SUMMERS, (1986)
J Phys. B 19 3479.

H P SUMMERS, M B HOOPER (1983)
Plasma Physics 25, 1344.

H P SUMMERS, P BRIDEN, W J DICKSON, J LANG, (1991)
'An Atomic Data & Analysis Structure for Spectral Emission in Laboratory and Astrophysical Plasmas' - to be published.

H P SUMMERS, L WOOD, (1988)
JET Joint Undertaking Report JET-R(88)06.

L A SVENSSON (1970)
Physica Scripta 1, 246.

P THOMAS (1990)
J. Nucl. Materials 176 and 177, 3.

A W WEISS (1972) Phys. Rev. A 6 1261.

W L WIESE, M W SMITH, B M GLENNON, (1966)
U S Dept of Commerce NSRDS-NBS4.

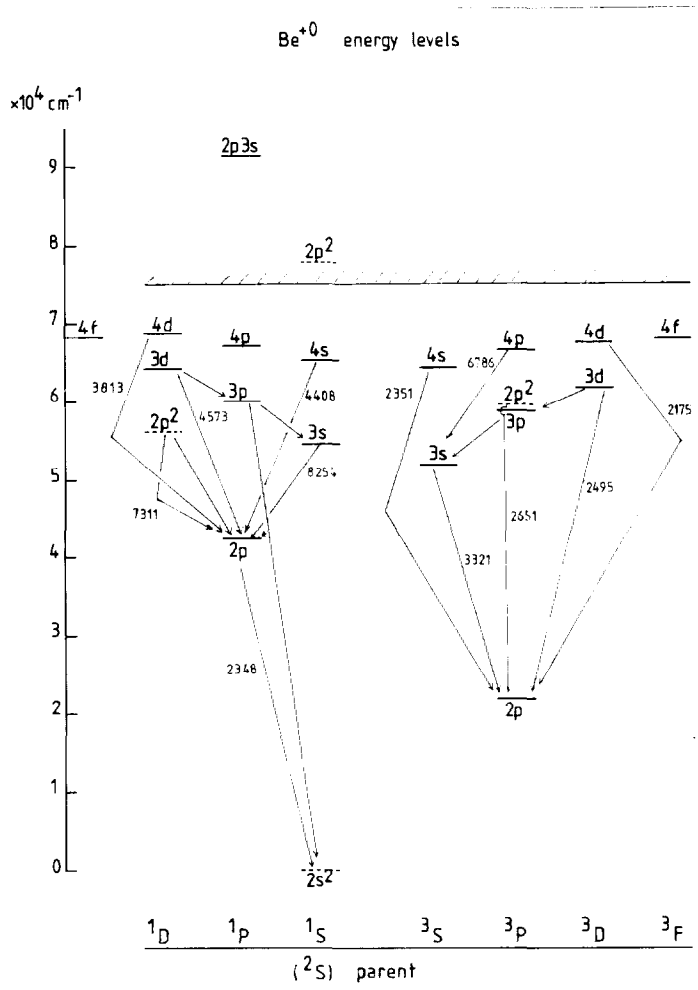

Figure 1 Energy level diagram for Be^{+0}.

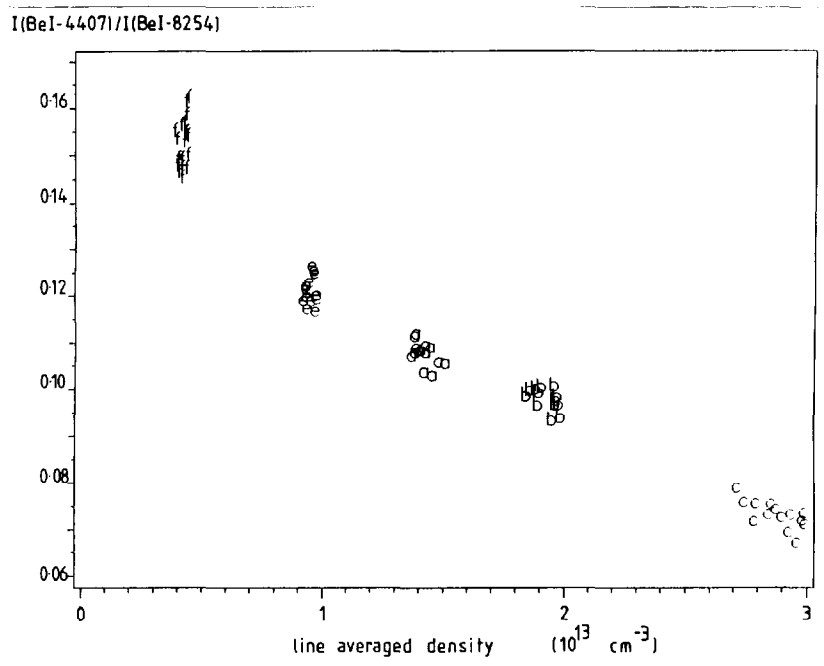

Figure 2 Variation of the ratio of observed photons emission in Be I 4408 Å and Be I 8254 Å with line averaged electron density for several JET pulses distinguished by alphabet letters. Line of sight directed at a beryllium/limiter.

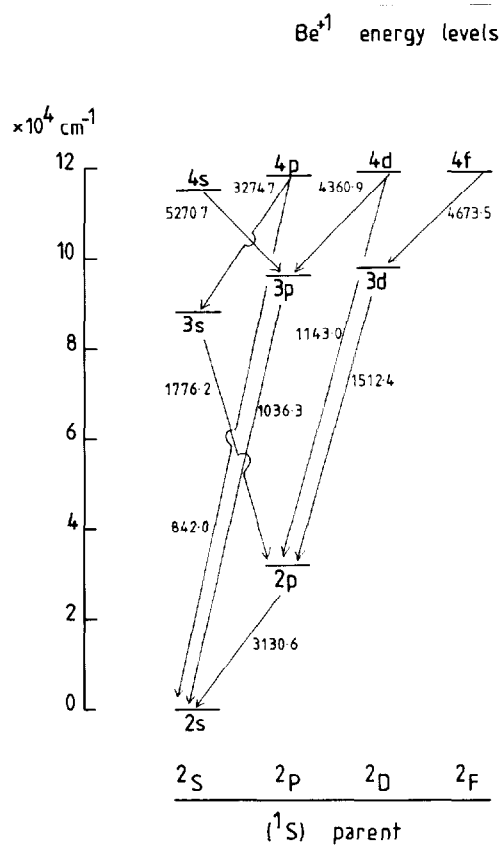

Figure 3 Energy level diagram for Be^{+1}.

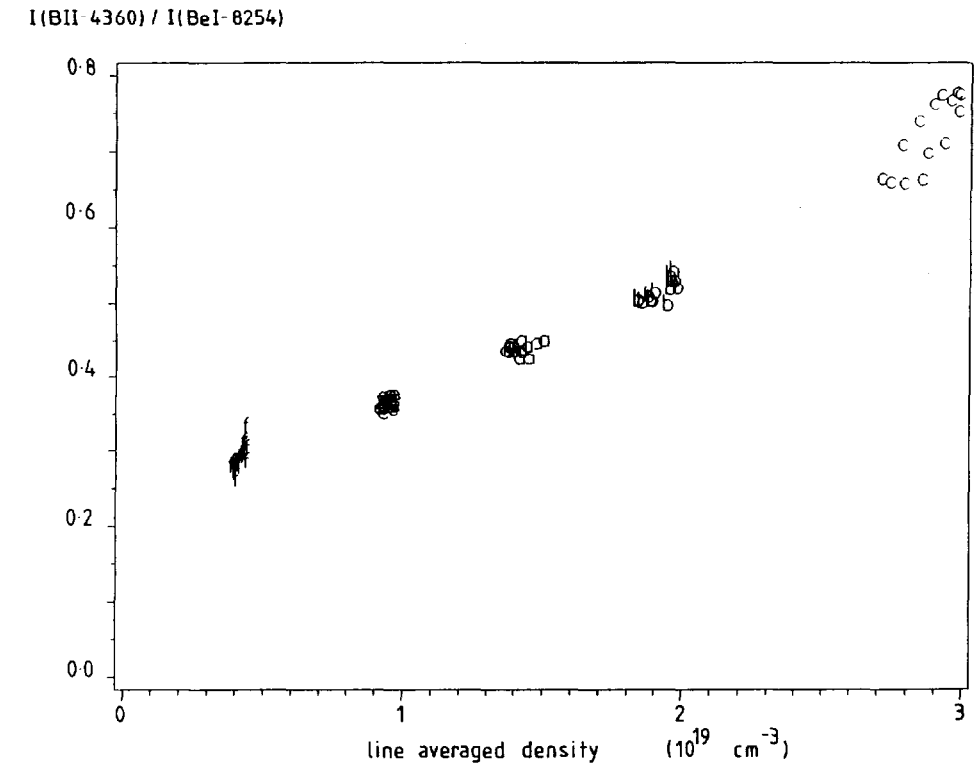

Figure 4 Variation of the ratio of observed photons emission in Be II 4360.9 and Be I 8254 Å with line averaged electron density. Line of sight directed at a beryllium limiter.

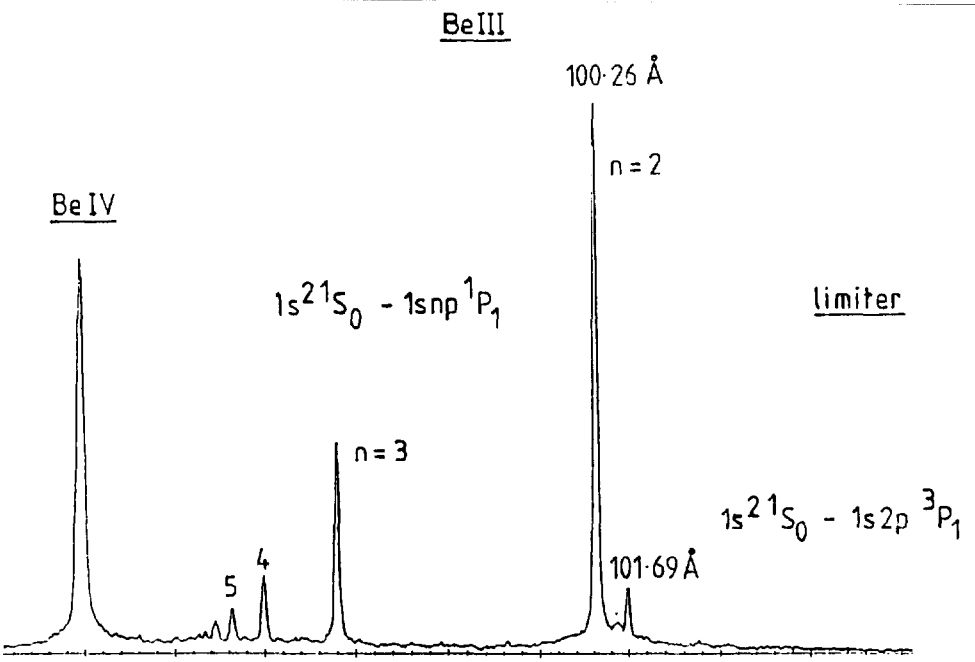

Figure 5 XUV spectrum identifying lines of Be III. Line of sight directed at inner wall in limiter phase.

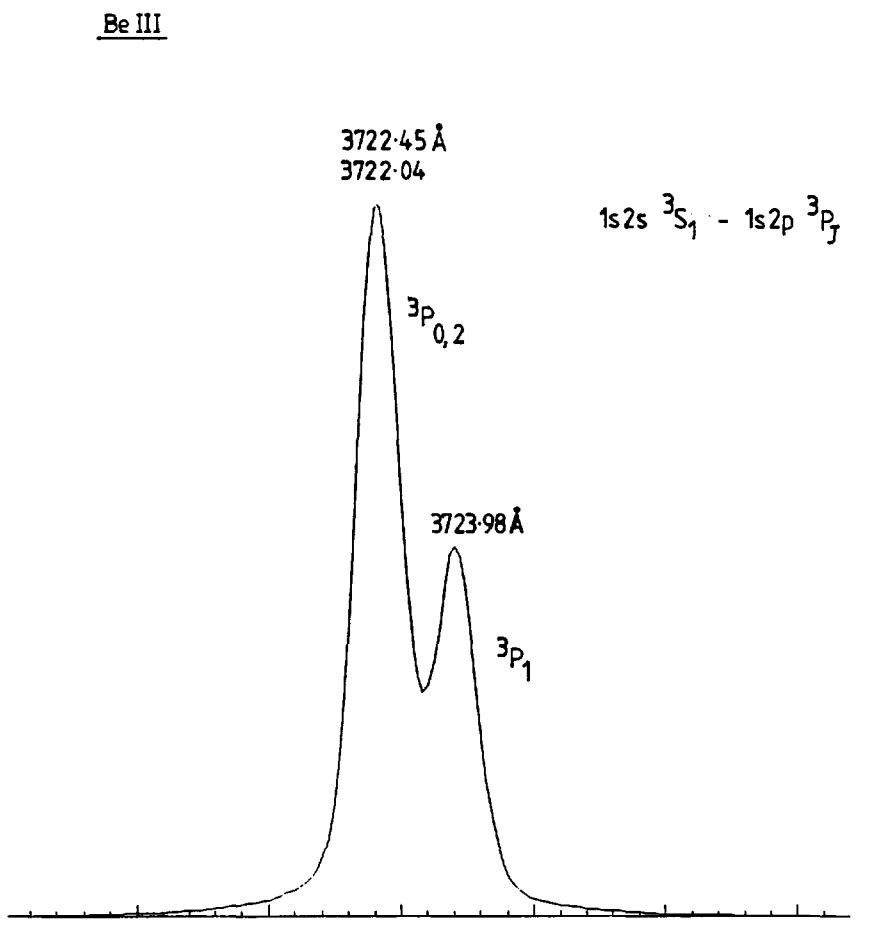

Figure 6 Spectral profile of Be III $1s2s\,{}^3S - 1s2p\,{}^3P$ multiplet.

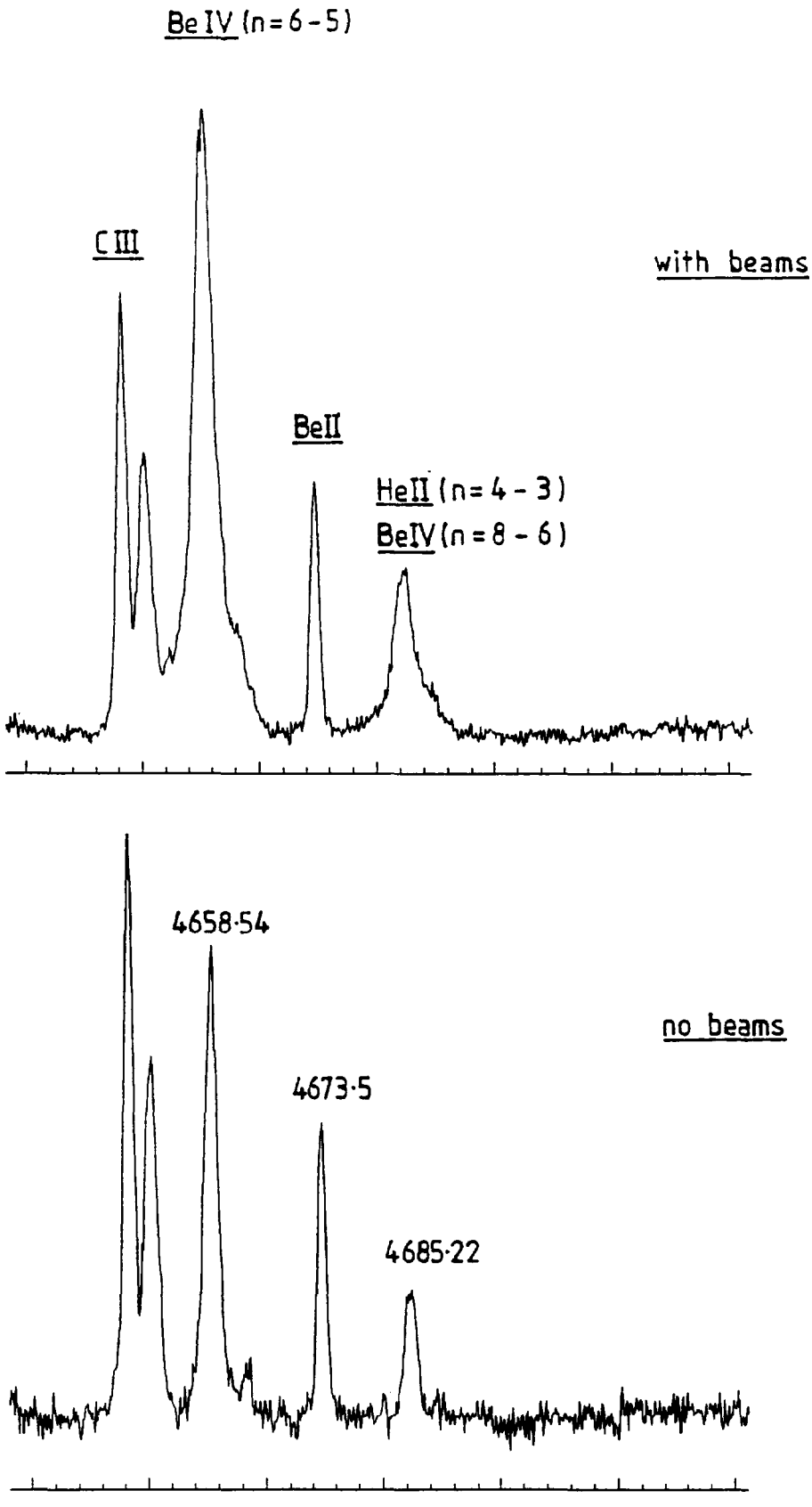

Figure 7a and 7b — Be IV n=6-5 and Be IV n=8-6 emission with and without neutral deuterium beam injection. Vertical line of sight through the beam line near the plasma centre.

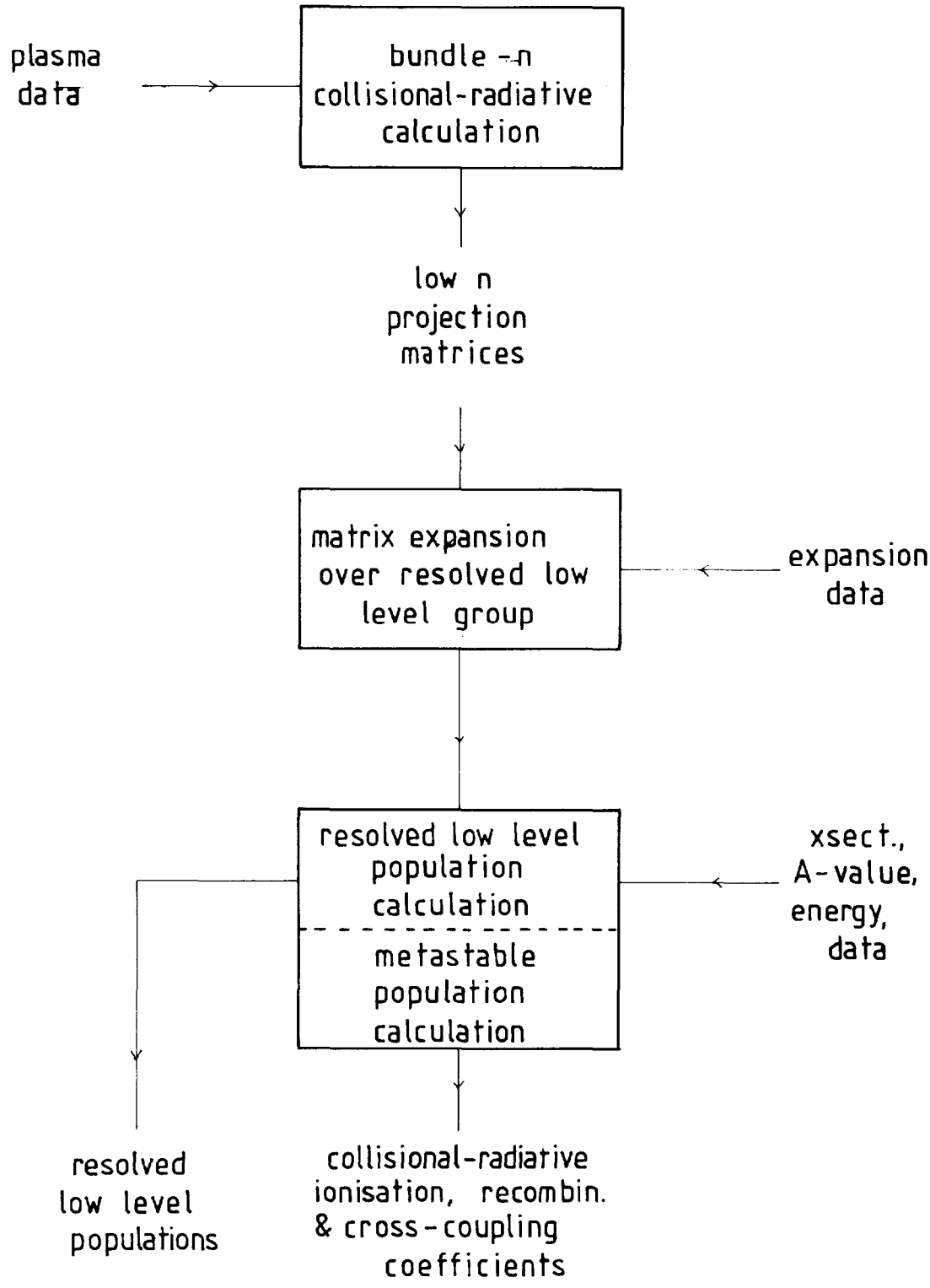

Figure 8 Schematic of population, emissivity and effective ionisation and recombination calculation for beryllium ions.

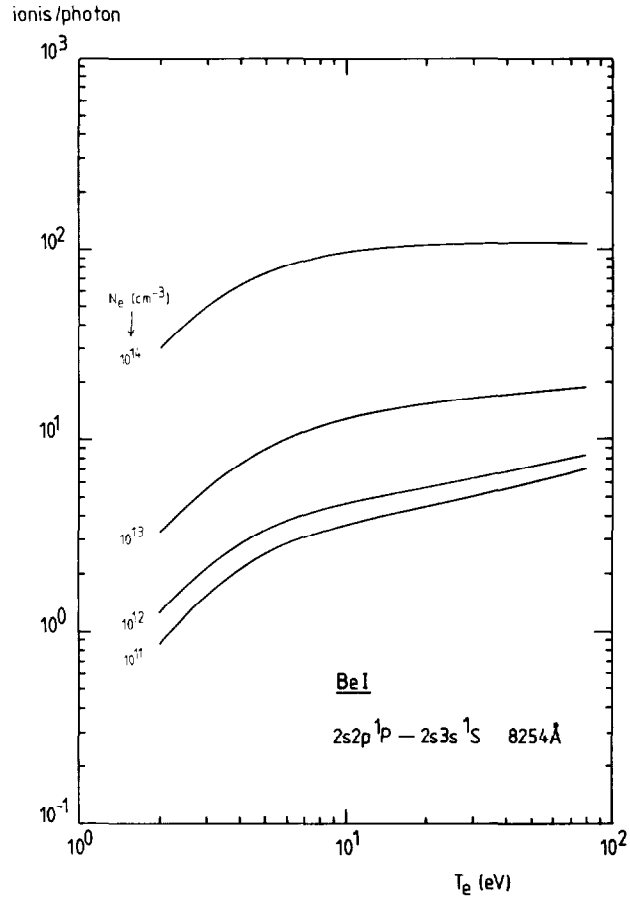

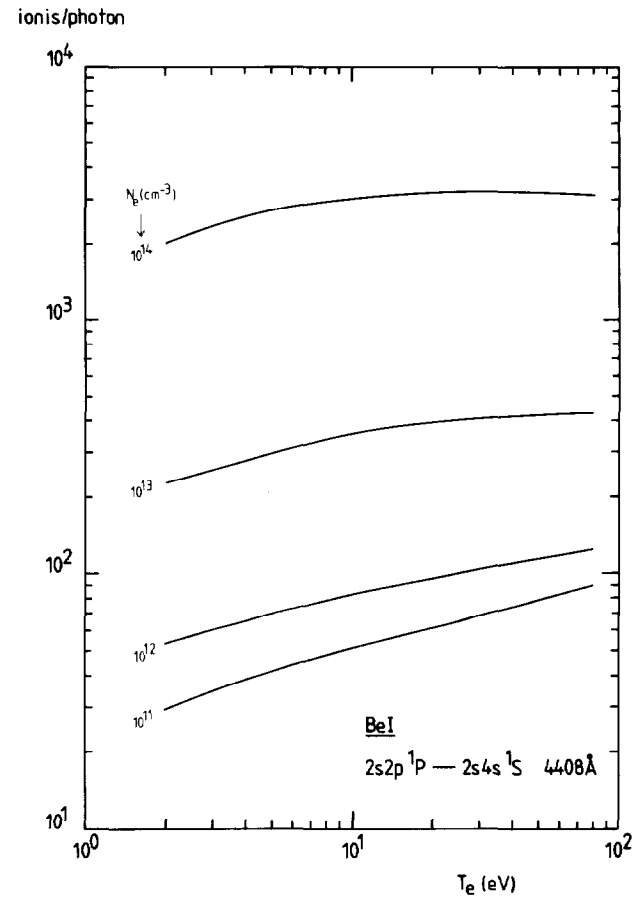

Figure 9a and 9b — Finite density ionisation per photon curves for Be I 8254 Å and Be I 4408 Å lines respectively.

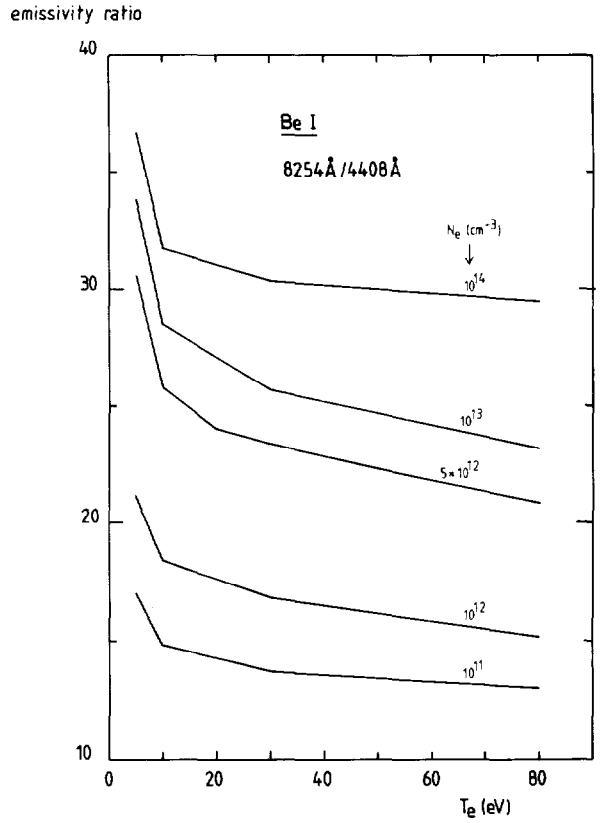

Figure 10 Variation of the emissivity ratio Be I 8254 Å/Be I 4408 Å with electron temperature and density.

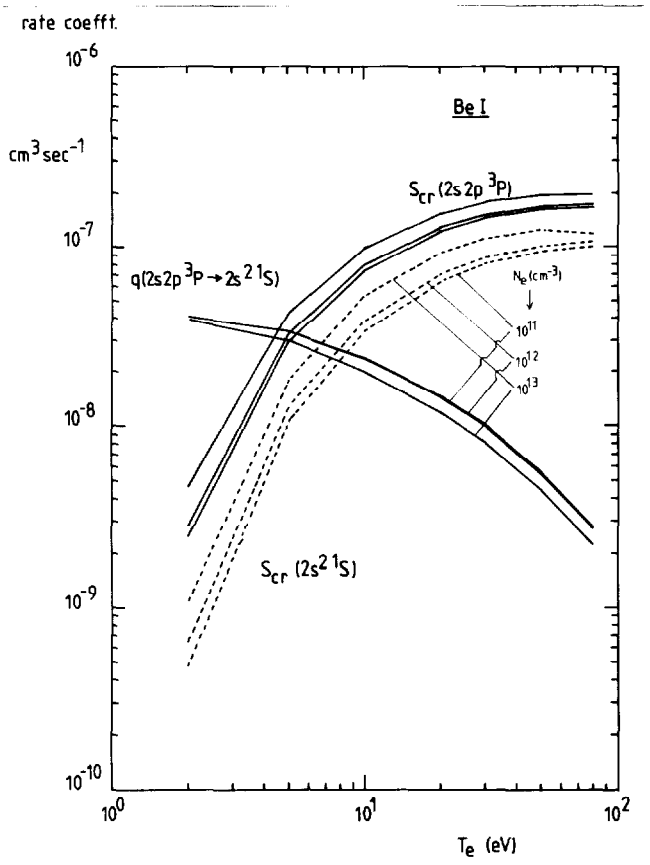

Figure 11 Generalised collisional-radiative coefficients for Be^{+0} ground and metastable states.

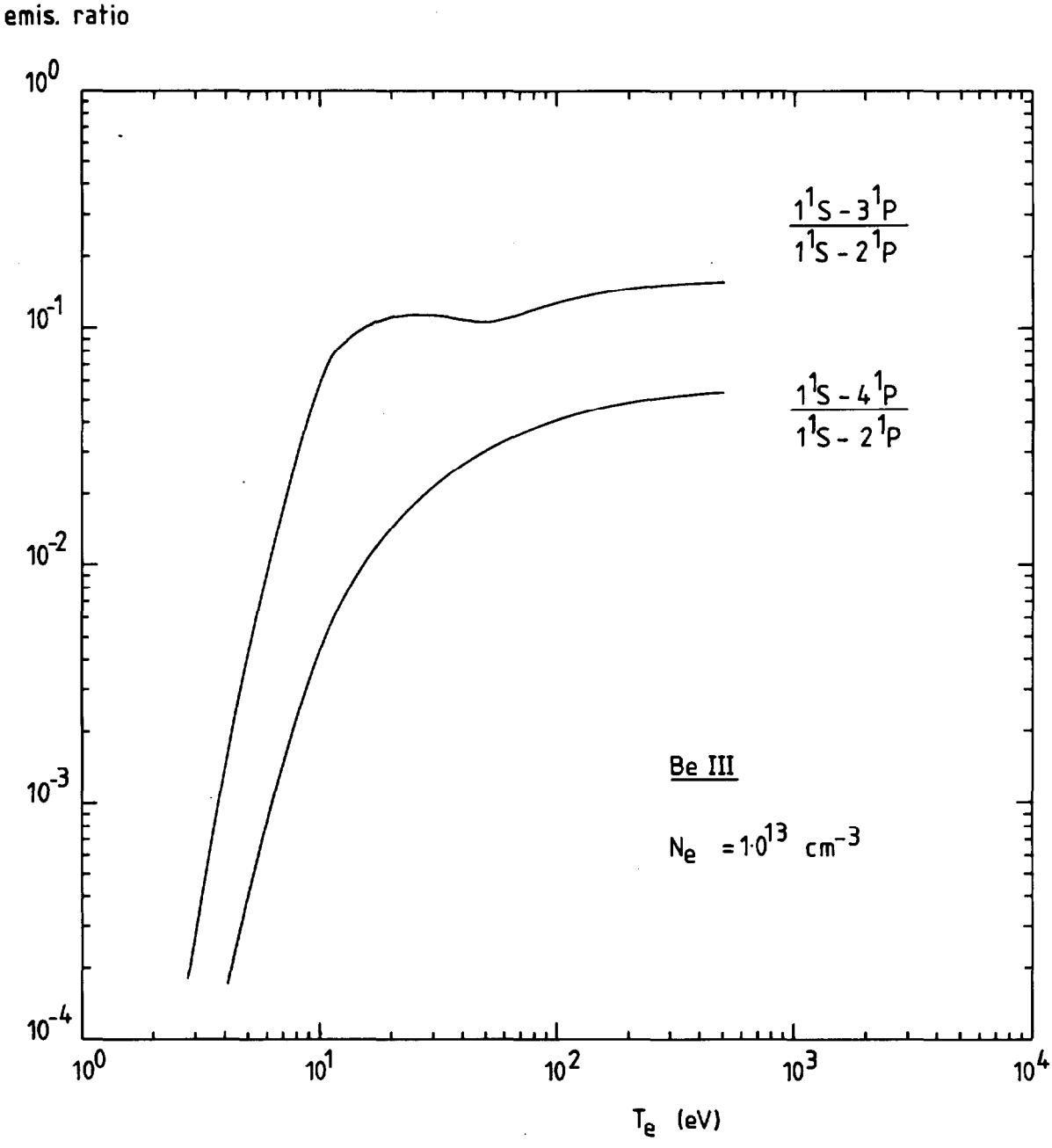

Figure 12 Calculated emissivity ratios Be III 1 ^{1}S - 3 ^{1}P/Be III 1 ^{1}S - 2P and Be III 1 ^{1}S - 4^{1}P/Be III 1 ^{1}S -2P.

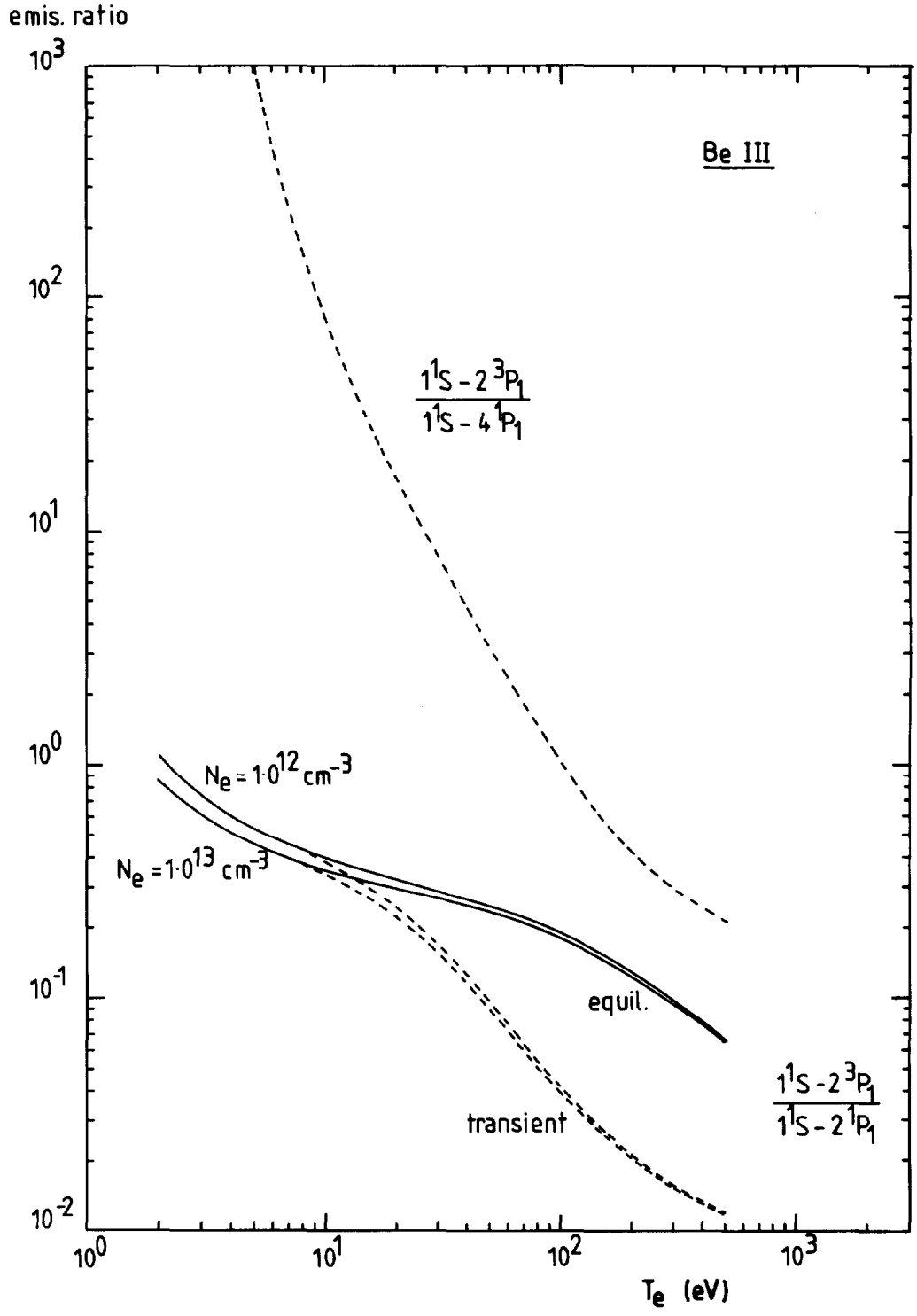

Figure 13 Emissivity ratios for Be III 1 $^1S_0$ - 2 $^3P_1$/Be III 1 $^1S_0$ - 2 $_1P_1$ in equilibrium (solid lines) and limiting transiently ionising (dashed lines) conditions, and for Be III 1 $^1S_0$ - 2 $^3P_1$/Be III 1 $^1S_0$ - 4 $^1P_1$ in limiting transiently ionising condition.

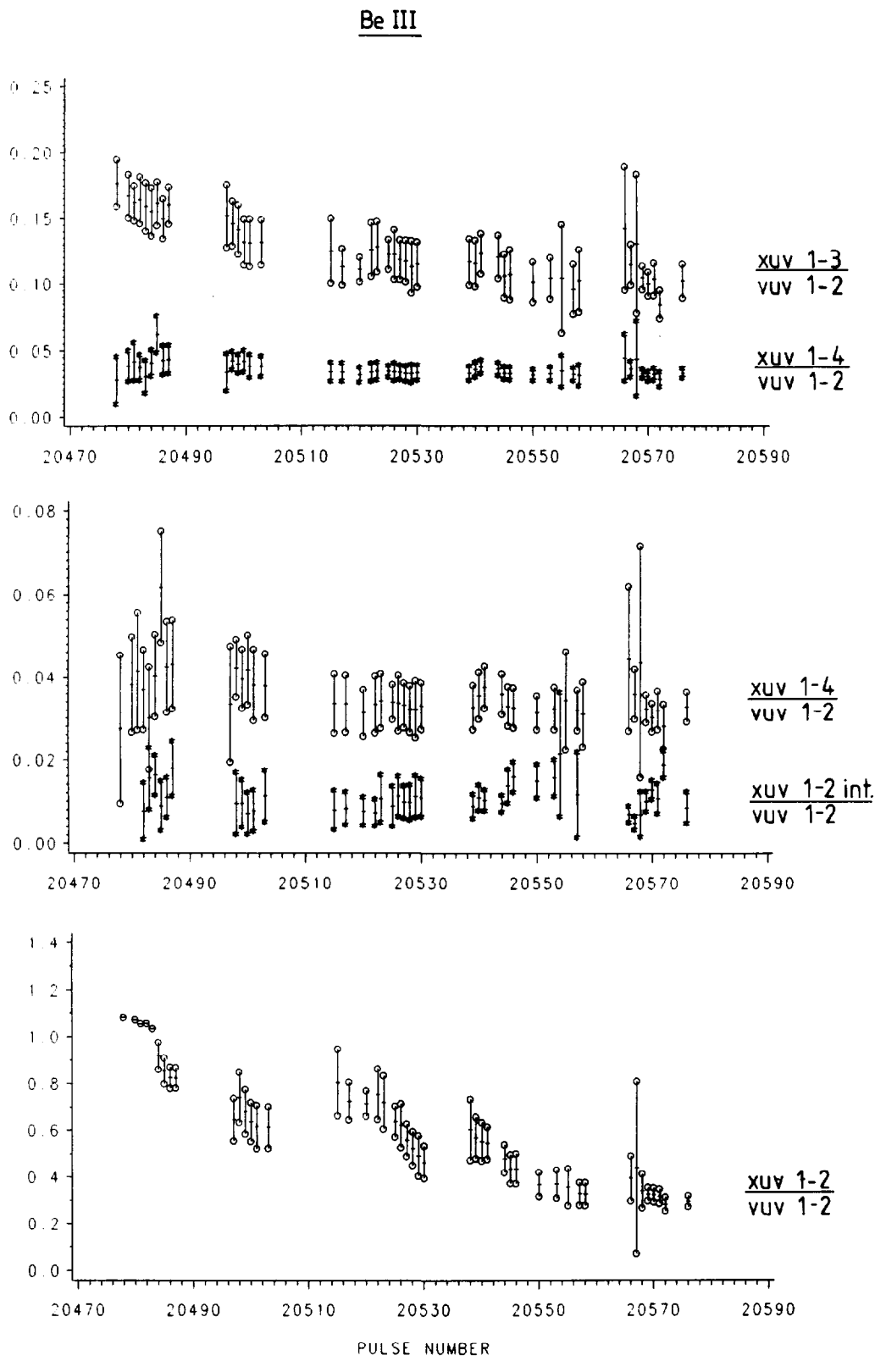

Figure 14 Evolution of XUV and VUV spectrometer comparison line ratios with JET pulse number, showing 'gain fatigue'.

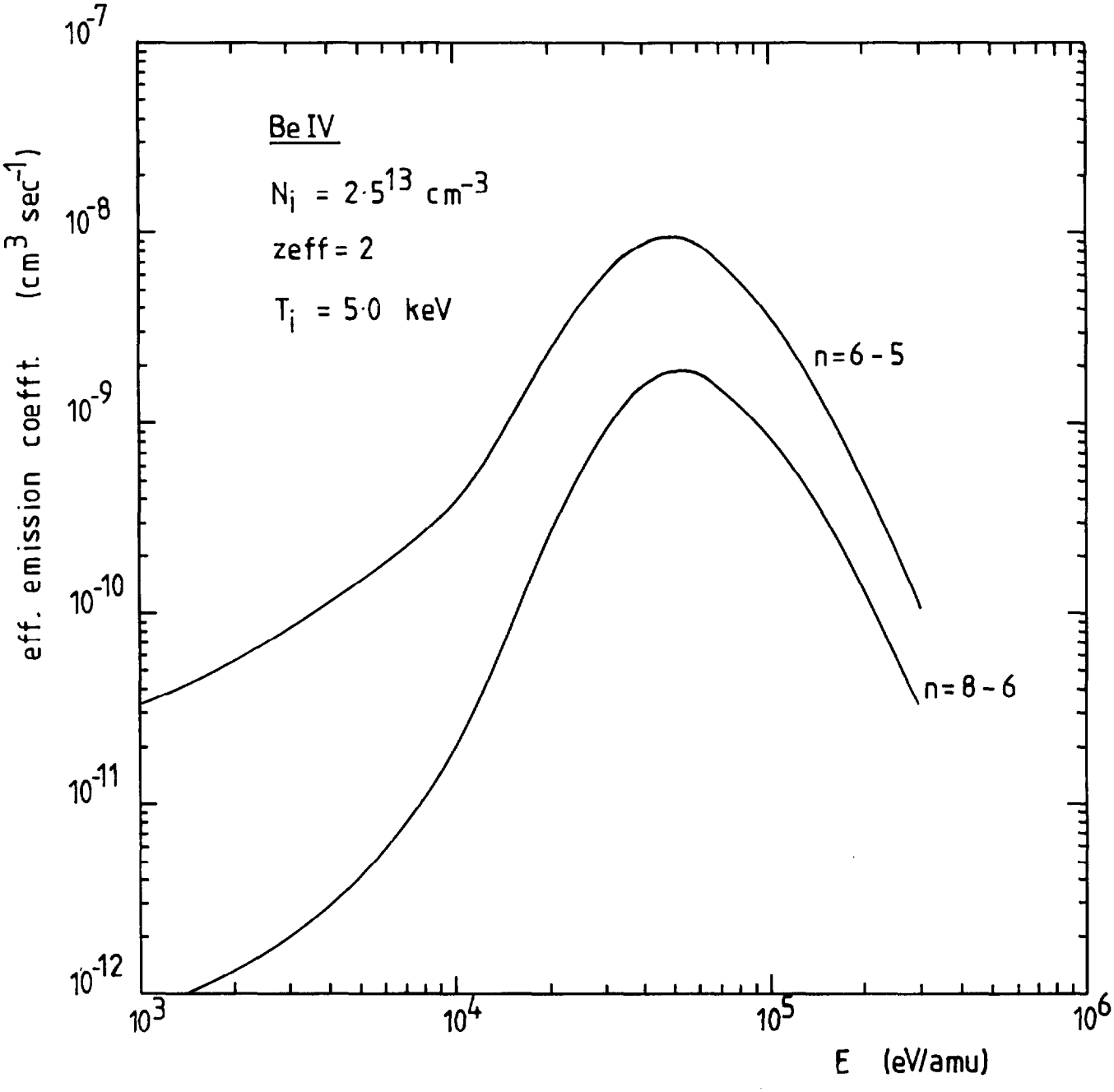

Figure 15 Effective emission coefficients for Be IV n = 6-5 and Be IV n = 8-6 as a function of incident deuterium beam energy following charge transfer.

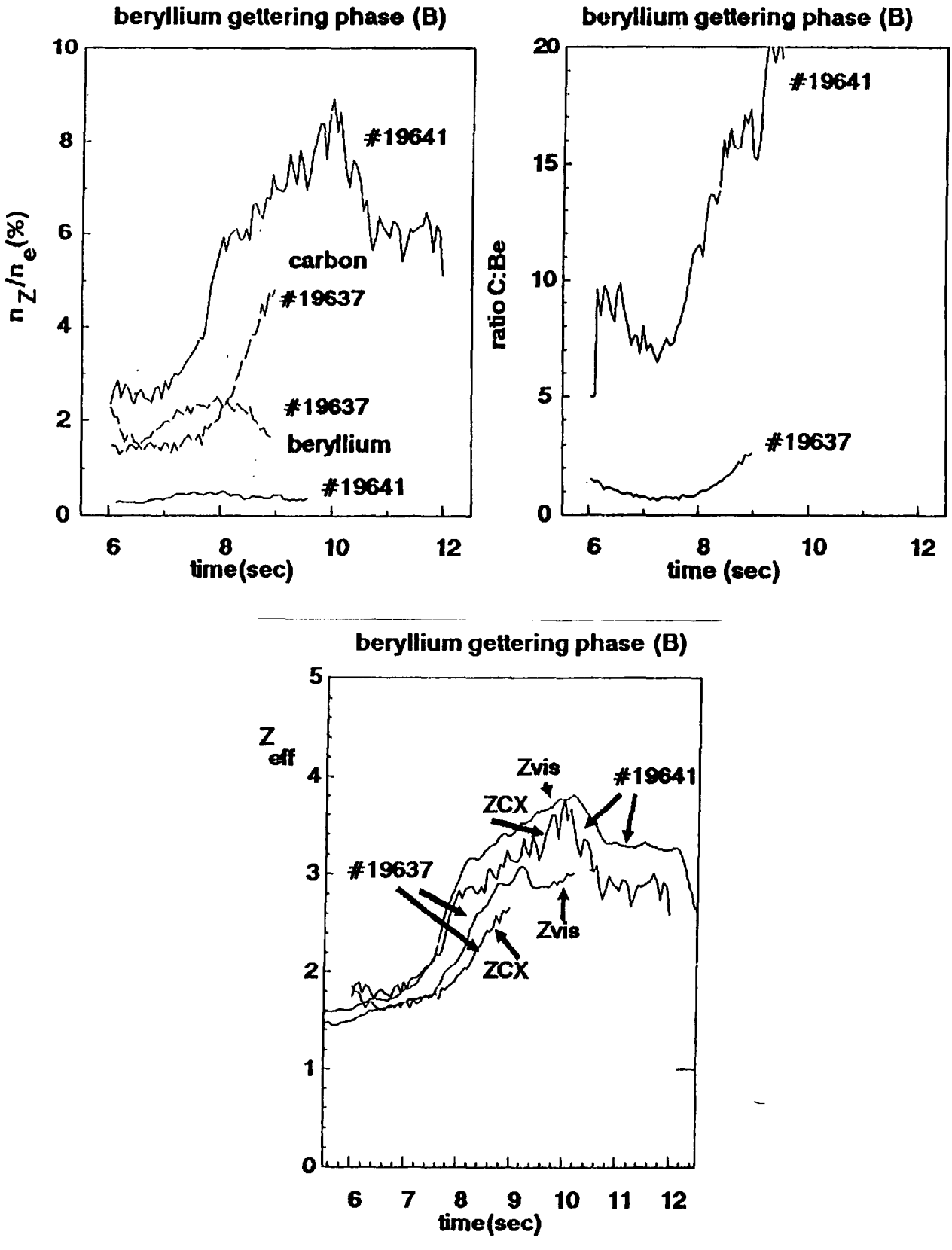

Figure 16 Evolution of carbon and beryllium densities and Z_{eff} in the JET beryllium evaporation phase.

Table 1

Theoretical transition probabilities for BeIII

Transition	A (sec^{-1})	Source
$2\ ^3S_1 - 2\ ^3P_1$	3.417^{7}	Schiff et al. (1971)
	3.57^{7}	Lin et al. (1977)
	3.42^{7}	Fernley et al. (1987)
	$\underline{3.57^{7}}$	
$1\ ^1S_0 - 2\ ^3P_1$	4.01^{5}	Drake & Dalgarno (1969)
	4.21^{5}	Lin et al. (1977)
	3.96^{5}	Safronova & Rudzikas (1977)
	3.99^{5}	Laughlin (1978)
	$\underline{4.23^{5}}$	

Branching ratio = 84.4 (+5.8/-3.6)

Summary of radiative transition probability data for Be III. Values adopted for the present analysis are underlined.

Table 2a

Ionisation per photon for BeI at 8254Å : 2s2p ^{1}P - 2s3s ^{1}S : 2s^2 ^{1}S metastable

N_e(cm^{-3})	1.00 ^{11}	1.00 ^{12}	5.00 ^{12}	1.00 ^{13}	1.00 ^{14}
T_e(eV)					
2.0 ^{0}	8.46 $^{-1}$	1.25	2.14	3.25	2.97 ^{1}
5.0 ^{0}	2.55	3.38	5.95	8.80	7.52 ^{1}
1.0 ^{1}	3.54	4.60	8.19	1.28 ^{1}	9.60 ^{1}
2.0 ^{1}	4.48	5.63	9.80	1.51 ^{1}	1.05 ^{2}
3.0 ^{1}	5.06	6.24	1.06 ^{1}	1.60 ^{1}	1.06 ^{2}
5.0 ^{1}	6.01	7.20	1.17 ^{1}	1.74 ^{1}	1.07 ^{2}
8.0 ^{1}	7.08	8.36	1.31 ^{1}	1.88 ^{1}	1.07 ^{2}

Ionisation per photon for BeI at 4408Å : 2s2p ^{1}P - 2s4s ^{1}S : 2s^2 ^{1}S metastable

N_e(cm^{-3})	1.00 ^{11}	1.00 ^{12}	5.00 ^{12}	1.00 ^{13}	1.00 ^{14}
T_e(eV)					
2.0 ^{0}	2.96 ^{1}	5.37 ^{1}	1.37 ^{2}	2.28 ^{2}	2.01 ^{3}
5.0 ^{0}	4.20 ^{1}	7.04 ^{1}	1.80 ^{2}	2.94 ^{2}	2.72 ^{3}
1.0 ^{1}	5.18 ^{1}	8.36 ^{1}	2.09 ^{2}	3.59 ^{2}	3.01 ^{3}
2.0 ^{1}	6.13 ^{1}	9.56 ^{1}	2.32 ^{2}	3.93 ^{2}	3.16 ^{3}
3.0 ^{1}	6.85 ^{1}	1.04 ^{2}	2.69 ^{2}	4.06 ^{2}	3.19 ^{3}
5.0 ^{1}	7.97 ^{1}	1.15 ^{2}	2.82 ^{2}	4.23 ^{2}	3.18 ^{3}
8.0 ^{1}	9.07 ^{1}	1.25 ^{2}	2.89 ^{2}	4.31 ^{2}	3.11 ^{3}

Ionisation per photon for BeI at 4573Å : 2s2p ^{1}P - 2s3d ^{1}D : 2s^2 ^{1}S metastable

N_e(cm^{-3})	1.00 ^{11}	1.00 ^{12}	1.00 ^{13}	1.00 ^{14}
T_e(eV)				
2.0 ^{0}	3.99	6.99	8.68	3.71 ^{1}
5.0 ^{0}	6.51	8.97	1.16 ^{1}	5.63 ^{1}
1.0 ^{1}	8.83	1.08 ^{1}	1.41 ^{1}	6.04 ^{1}
2.0 ^{1}	1.19 ^{1}	1.33 ^{1}	1.59 ^{1}	6.06 ^{1}
3.0 ^{1}	1.42 ^{1}	1.54 ^{1}	1.70 ^{1}	5.90 ^{1}
5.0 ^{1}	1.77 ^{1}	1.87 ^{1}	1.87 ^{1}	5.68 ^{1}
8.0 ^{1}	2.10 ^{1}	2.21 ^{1}	2.02 ^{1}	5.52 ^{1}

Table 2b

Ionisation per photon for BeII at 3131Å : $2s\ ^2S - 2p\ ^2P$: $2s\ ^2S$ metastable

$N_e(cm^{-3})$ / $T_e(eV)$	1.00^{11}	2.00^{11}	5.00^{11}	1.00^{12}	2.00^{12}	5.00^{12}	1.00^{13}	2.00^{13}	5.00^{13}	1.00^{14}
5.0^{0}	1.86^{-3}	1.86^{-3}	1.86^{-3}	1.86^{-3}	1.86^{-3}	1.86^{-3}	1.88^{-3}	1.90^{-3}	1.96^{-3}	2.07^{-3}
1.0^{1}	1.03^{-2}	1.03^{-2}	1.03^{-2}	1.03^{-2}	1.03^{-2}	1.04^{-2}	1.04^{-2}	1.05^{-2}	1.08^{-2}	1.14^{-2}
2.0^{1}	2.65^{-2}	2.65^{-2}	2.65^{-2}	2.66^{-2}	2.66^{-2}	2.66^{-2}	2.67^{-2}	2.70^{-2}	2.76^{-2}	2.89^{-2}
5.0^{1}	5.05^{-2}	5.05^{-2}	5.05^{-2}	5.05^{-2}	5.05^{-2}	5.05^{-2}	5.08^{-2}	5.11^{-2}	5.24^{-2}	5.42^{-2}
1.0^{2}	6.69^{-2}	6.69^{-2}	6.69^{-2}	6.70^{-2}	6.70^{-2}	6.70^{-2}	6.70^{-2}	6.75^{-2}	6.88^{-2}	7.09^{-2}
2.0^{2}	7.94^{-2}	7.94^{-2}	7.94^{-2}	7.94^{-2}	7.94^{-2}	7.94^{-2}	7.94^{-2}	8.03^{-2}	8.13^{-2}	8.33^{-2}

Ionisation per photon for BeII at 5271Å : $3p\ ^2P - 4s\ ^2S$: $2s\ ^2S$ metastable

$N_e(cm^{-3})$ / $T_e(eV)$	1.00^{11}	2.00^{11}	5.00^{11}	1.00^{12}	2.00^{12}	5.00^{12}	1.00^{13}	2.00^{13}	5.00^{13}	1.00^{14}
5.0^{0}	6.24	6.23	6.31	6.37	6.52	6.91	7.53	8.42	9.45	8.98
1.0^{1}	1.44^{1}	1.45^{1}	1.45^{1}	1.47^{1}	1.50^{1}	1.59^{1}	1.72^{1}	1.91^{1}	2.11^{1}	1.98^{1}
2.0^{1}	2.16^{1}	2.17^{1}	2.18^{1}	2.20^{1}	2.25^{1}	2.37^{1}	2.56^{1}	2.84^{1}	3.19^{1}	3.07^{1}
5.0^{1}	2.95^{1}	2.96^{1}	2.97^{1}	2.99^{1}	3.04^{1}	3.17^{1}	3.37^{1}	3.70^{1}	4.21^{1}	4.23^{1}
1.0^{2}	3.52^{1}	3.52^{1}	3.53^{1}	3.54^{1}	3.58^{1}	3.68^{1}	3.84^{1}	4.14^{1}	4.70^{1}	4.85^{1}
2.0^{2}	3.97^{1}	3.97^{1}	3.98^{1}	3.98^{1}	4.00^{1}	4.06^{1}	4.19^{1}	4.45^{1}	5.00^{1}	5.28^{1}

Ionisation per photon for BeII at 4674Å : 3d ^{2}D - 4f ^{2}F : 2s ^{2}S metastable

$N_e(cm^{-3})$	1.00 ^{11}	2.00 ^{11}	5.00 ^{11}	1.00 ^{12}	2.00 ^{12}	5.00 ^{12}	1.00 ^{13}	2.00 ^{13}	5.00 ^{13}	1.00 ^{14}
T_e(eV)										
5.0 ^{0}	2.31	2.30	2.29	2.27	2.22	2.07	1.88	1.61	1.18	8.57 $^{-1}$
1.0 ^{1}	5.15	5.12	5.08	5.03	4.90	4.54	4.11	3.49	2.53	1.79
2.0 ^{1}	9.14	9.13	9.03	8.91	8.64	7.94	7.08	5.88	4.14	2.86
5.0 ^{1}	1.85 ^{1}	1.84 ^{1}	1.82 ^{1}	1.78 ^{1}	1.72 ^{1}	1.55 ^{1}u	1.33 ^{1}	1.06 ^{1}	6.87	4.54
1.0 ^{2}	2.94 ^{1}	2.93 ^{1}	2.89 ^{1}	2.82 ^{1}	2.70 ^{1}	2.39 ^{1}	2.01 ^{1}	1.54 ^{1}	9.48	6.03
2.0 ^{2}	4.02 ^{1}	4.02 ^{1}	3.97 ^{1}	3.89 ^{1}	3.73 ^{1}	3.33 ^{1}	2.78 ^{1}	2.11 ^{1}	1.26 ^{1}	7.86

Ionisation per photon for BeII at 4361Å : 3p ^{2}P - 4d ^{2}D : 2s ^{2}S metastable

$N_e(cm^{-3})$	1.00 ^{11}	2.00 ^{11}	5.00 ^{11}	1.00 ^{12}	2.00 ^{12}	5.00 ^{12}	1.00 ^{13}	2.00 ^{13}	5.00 ^{13}	1.00 ^{14}
T_e(eV)										
5.0 ^{0}	6.30	6.27	6.17	6.04	5.80	5.37	4.89	4.27	3.28	2.42
1.0 ^{1}	1.24 ^{1}	1.23 ^{1}	1.22 ^{1}	1.20 ^{1}	1.17 ^{1}	1.10 ^{1}	1.02 ^{1}	8.98	6.85	5.02
2.0 ^{1}	1.88 ^{1}	1.88 ^{1}	1.86 ^{1}	1.85 ^{1}	1.80 ^{1}	1.71 ^{1}	1.59 ^{1}	1.41 ^{1}	1.08 ^{1}	7.91
5.0 ^{1}	2.78 ^{1}	2.78 ^{1}	2.77 ^{1}	2.73 ^{1}	2.67 ^{1}	2.52 ^{1}	2.33 ^{1}	2.08 ^{1}	1.61 ^{1}	1.19 ^{1}
1.0 ^{2}	3.52 ^{1}	3.51 ^{1}	3.48 ^{1}	3.43 ^{1}	3.34 ^{1}	3.13 ^{1}	2.88 ^{1}	2.55 ^{1}	1.98 ^{1}	1.48 ^{1}
2.0 ^{2}	4.25 ^{1}	4.24 ^{1}	4.19 ^{1}	4.13 ^{1}	4.01 ^{1}	3.72 ^{1}	3.40 ^{1}	2.99 ^{1}	2.35 ^{1}	1.78 ^{1}

Table 3

Effective emission coefficients for BeIV (n = 6-5) at 4657Å

Reference $q_{eff} = 8.56^{-9}$ ($cm^3\ sec^{-1}$) at $E_{beam} = 4.0^4$ (eV/amu), $T_I = 5.0^3$ (eV), $N_I = 2.5^{13}$ (cm^{-3}), $Z_{eff} = 2$

E_{beam}	q_{eff}	E_{beam}	q_{eff}	N_I	q_{eff}	T_I	q_{eff}	Z_{eff}	q_{eff}
1.0^3	3.26^{-11}	4.0^4	8.56^{-9}	1.0^3	7.87^{-9}	1.0^{11}	1.17^{-8}	1.0	1.03^{-8}
1.5^3	4.24^{-11}	5.0^4	9.43^{-9}	2.0^3	8.14^{-9}	2.0^{11}	1.18^{-8}	2.0	8.56^{-9}
2.0^3	5.46^{-11}	6.0^4	8.73^{-9}	3.0^3	8.32^{-9}	5.0^{11}	1.18^{-8}	3.0	7.67^{-9}
3.0^3	7.98^{-11}	7.0^4	6.99^{-9}	5.0^3	8.56^{-9}	1.0^{12}	1.17^{-8}	4.0	7.22^{-9}
5.5^3	1.62^{-10}	8.0^4	5.63^{-9}	7.0^3	8.73^{-9}	2.0^{12}	1.15^{-8}	5.0	6.96^{-9}
7.0^3	2.18^{-10}	1.0^5	3.69^{-9}	1.0^4	8.92^{-9}	5.0^{12}	1.07^{-8}	6.0	6.81^{-9}
1.0^4	3.67^{-10}	1.5^5	1.27^{-9}	1.3^4	9.06^{-9}	1.0^{13}	9.85^{-8}		
1.5^4	1.04^{-9}	2.0^5	4.87^{-10}	1.6^4	9.17^{-9}	2.0^{13}	8.87^{-9}		
2.0^4	2.33^{-9}	3.0^5	1.06^{-10}	1.9^4	9.27^{-9}	5.0^{13}	7.74^{-9}		
3.0^4	5.84^{-9}			2.2^4	9.35^{-9}	1.0^{14}	7.15^{-9}		
				2.5^4	9.42^{-9}				
				3.0^4	9.52^{-9}				

Charge exchange induced effective emission coefficients for Be IV n= 6 - 5 from D(1s).

APPENDIX 1.

THE JET TEAM

JET Joint Undertaking, Abingdon, Oxon, OX14 3EA, U.K.

J.M.Adams[1], F.Alladio[4], H.Altmann, R.J.Anderson, G.Appruzzese, W.Bailey, B.Balet, D.V.Bartlett, L.R.Baylor[24], K.Behringer, A.C.Bell, P.Bertoldi, E.Bertolini, V.Bhatnagar, R.J.Bickerton, A.Boileau[3], T.Bonicelli, S.J.Booth, G.Bosia, M.Botman, D.Boyd[31], H.Brelen, H.Brinkschulte, M.Brusati, T.Budd, M.Bures, T.Businaro[4], H.Buttgereit, D.Cacaut, C.Caldwell-Nichols, D.J.Campbell, P.Card, J.Carwardine, G.Celentano, P.Chabert[27], C.D.Challis, A.Cheetham, J.Christiansen, C.Christodoulopoulos, P.Chuilon, R.Claesen, S.Clement[30], J.P.Coad, P.Colestock[6], S.Conroy[13], M.Cooke, S.Cooper, J.G.Cordey, W.Core, S.Corti, A.E.Costley, G.Cottrell, M.Cox[7], P.Cripwell[13], F.Crisanti[4], D.Cross, H.de Blank[16], J.de Haas[16], L.de Kock, E.Deksnis, G.B.Denne, G.Deschamps, G.Devillars, K.J.Dietz, J.Dobbing, S.E.Dorling, P.G.Doyle, D.F.Düchs, H.Duquenoy, A.Edwards, J.Ehrenberg[14], T.Elevant[12], W.Engelhardt, S.K.Erents[7], L.G.Eriksonn[5], M.Evrard[2], H.Falter, D.Flory, M.Forrest[7], C.Froger, K.Fullard, M.Gadeberg[11], A.Galetsas, R.Galvao[8], A.Gibson, R.D.Gill, A.Gondhalekar, C.Gordon, G.Gorini, C.Gormezano, N.A.Gottardi, C.Gowers, B.J.Green, F.S.Griph, M.Gryzinski[26], R.Haange, G.Hammett[6], W.Han[9], C.J.Hancock, P.J.Harbour, N.C.Hawkes[7], P.Haynes[7], T.Hellsten, J.L.Hemmerich, R.Hemsworth, R.F.Herzog, K.Hirsch[14], J.Hoekzema, W.A.Houlberg[24], J.How, M.Huart, A.Hubbard, T.P.Hughes[32], M.Hugon, M.Huguet, J.Jacquinot, O.N.Jarvis, T.C.Jernigan[24], E.Joffrin, E.M.Jones, L.P.D.F.Jones, T.T.C.Jones, J.Källne, A.Kaye, B.E.Keen, M.Keilhacker, G.J.Kelly, A.Khare[15], S.Knowlton, A.Konstantellos, M.Kovanen[21], P.Kupschus, P.Lallia, J.R.Last, L.Lauro-Taroni, M.Laux[33], K.Lawson[7], E.Lazzaro, M.Lennholm, X.Litaudon, P.Lomas, M.Lorentz-Gottardi[2], C.Lowry, G.Magyar, D.Maisonnier, M.Malacarne, V.Marchese, P.Massmann, L.McCarthy[28], G.McCracken[7], P.Mendonca, P.Meriguet, P.Micozzi[4], S.F.Mills, P.Millward, S.L.Milora[24], A.Moissonnier, P.L.Mondino, D.Moreau[17], P.Morgan, H.Morsi[14], G.Murphy, M.F.Nave, M.Newman, L.Nickesson, P.Nielsen, P.Noll, W.Obert, D.O'Brien, J.O'Rourke, M.G.Pacco-Düchs, M.Pain, S.Papastergiou, D.Pasini[20], M.Paume[27], N.Peacock[7], D.Pearson[13], F.Pegoraro, M.Pick, S.Pitcher[7], J.Plancoulaine, J-P.Poffé, F.Porcelli, R.Prentice, T.Raimondi, J.Ramette[17], J.M.Rax[27], C.Raymond, P-H.Rebut, J.Removille, F.Rimini, D.Robinson[7], A.Rolfe, R.T.Ross, L.Rossi, G.Rupprecht[14], R.Rushton, P.Rutter, H.C.Sack, G.Sadler, N.Salmon[13], H.Salzmann[14], A.Santagiustina, D.Schissel[25], P.H.Schild, M.Schmid, G.Schmidt[6], R.L.Shaw, A.Sibley, R.Simonini, J.Sips[16], P.Smeulders, J.Snipes, S.Sommers, L.Sonnerup, K.Sonnenberg, M.Stamp, P.Stangeby[19], D.Start, C.A.Steed, D.Stork, P.E.Stott, T.E.Stringer, D.Stubberfield, T.Sugie[18], D.Summers, H.Summers[20], J.Taboda-Duarte[22], J.Tagle[30], H.Tamnen, A.Tanga, A.Taroni, C.Tebaldi[23], A.Tesini, P.R.Thomas, E.Thompson, K.Thomsen[11], P.Trevalion, M.Tschudin, B.Tubbing, K.Uchino[29], E.Usselmann, H.van der Beken, M.von Hellermann, T.Wade, C.Walker, B.A.Wallander, M.Walravens, K.Walter, D.Ward, M.L.Watkins, J.Wesson, D.H.Wheeler, J.Wilks, U.Willen[12], D.Wilson, T.Winkel, C.Woodward, M.Wykes, I.D.Young, L.Zannelli, M.Zarnstorff[6], D.Zasche[14], J.W.Zwart.

PERMANENT ADDRESS

1. UKAEA, Harwell, Oxon. UK.
2. EUR-EB Association, LPP-ERM/KMS, B-1040 Brussels, Belgium.
3. Institute National des Récherches Scientifique, Quebec, Canada.
4. ENEA-CENTRO Di Frascati, I-00044 Frascati, Roma, Italy.
5. Chalmers University of Technology, Göteborg, Sweden.
6. Princeton Plasma Physics Laboratory, New Jersey, USA.
7. UKAEA Culham Laboratory, Abingdon, Oxon. UK.
8. Plasma Physics Laboratory, Space Research Institute, Sao José dos Campos, Brazil.
9. Institute of Mathematics, University of Oxford, UK.
10. CRPP/EPFL, 21 Avenue des Bains, CH-1007 Lausanne, Switzerland.
11. Risø National Laboratory, DK-4000 Roskilde, Denmark.
12. Swedish Energy Research Commission, S-10072 Stockholm, Sweden.
13. Imperial College of Science and Technology, University of London, UK.
14. Max Planck Institut für Plasmaphysik, D-8046 Garching bei München, FRG.
15. Institute for Plasma Research, Gandhinagar Bhat Gujat, India.
16. FOM Instituut voor Plasmafysica, 3430 Be Nieuwegein, The Netherlands.
17. Commissiariat à L'Energie Atomique, F-92260 Fontenay-aux-Roses, France.
18. JAERI, Tokai Research Establishment, Tokai-Mura, Naka-Gun, Japan.
19. Institute for Aerospace Studies, University of Toronto, Downsview, Ontario, Canada.
20. University of Strathclyde, Glasgow, G4 ONG, U.K.
21. Nuclear Engineering Laboratory, Lapeenranta University, Finland.
22. JNICT, Lisboa, Portugal.
23. Department of Mathematics, Univeristy of Bologna, Italy.
24. Oak Ridge National Laboratory, Oak Ridge, Tenn., USA.
25. G.A. Technologies, San Diego, California, USA.
26. Institute for Nuclear Studies, Swierk, Poland.
27. Commissiariat à l'Energie Atomique, Cadarache, France.
28. School of Physical Sciences, Flinders University of South Australia, South Australia SO42.
29. Kyushi University, Kasagu Fukuoka, Japan.
30. Centro de Investigaciones Energeticas Medioambientales y Techalogicas, Spain.
31. University of Maryland, College Park, Maryland, USA.
32. University of Essex, Colchester, UK.
33. Akademie de Wissenschaften, Berlin, DDR.

CR 88.49.1A